


2023

## Material Characterization of Thermoplastic Polyurethane (TPU) and Thermoplastic Elastomers (TPE) for Development of 3D-Printed Surrogate Organs for Medical Training

Anastasia Elizabeth Lucci  
West Virginia University, ael00004@mix.wvu.edu

Follow this and additional works at: <https://researchrepository.wvu.edu/etd>

 Part of the [Anatomy Commons](#), [Biomedical Engineering and Bioengineering Commons](#), [Manufacturing Commons](#), [Materials Science and Engineering Commons](#), and the [Medical Education Commons](#)

---

### Recommended Citation

Lucci, Anastasia Elizabeth, "Material Characterization of Thermoplastic Polyurethane (TPU) and Thermoplastic Elastomers (TPE) for Development of 3D-Printed Surrogate Organs for Medical Training" (2023). *Graduate Theses, Dissertations, and Problem Reports*. 12241.  
<https://researchrepository.wvu.edu/etd/12241>

This Thesis is protected by copyright and/or related rights. It has been brought to you by the The Research Repository @ WVU with permission from the rights-holder(s). You are free to use this Thesis in any way that is permitted by the copyright and related rights legislation that applies to your use. For other uses you must obtain permission from the rights-holder(s) directly, unless additional rights are indicated by a Creative Commons license in the record and/ or on the work itself. This Thesis has been accepted for inclusion in WVU Graduate Theses, Dissertations, and Problem Reports collection by an authorized administrator of The Research Repository @ WVU. For more information, please contact [researchrepository@mail.wvu.edu](mailto:researchrepository@mail.wvu.edu).

**Material Characterization of  
Thermoplastic Polyurethane (TPU) and Thermoplastic Elastomers (TPE)  
for Development of 3D-Printed Surrogate Organs for Medical Training**

**Anastasia Elizabeth Lucci**

Thesis submitted to the Benjamin M. Statler College of Engineering and Mineral Resources at  
West Virginia University

in partial fulfillment of the requirements for the degree of

Master of Sciences

in

Mechanical Engineering

Eduardo M. Sosa, Ph.D., Chair

Gregory J. Thompson, Ph.D.

Ever J. Barbero, Ph.D.

Bruce Palmer

Department of Mechanical, Materials, and Aerospace Engineering

Morgantown, West Virginia

December 2023

Keywords: Thermoplastic Polyurethanes, Thermoplastic Elastomers, Surrogate Organs, 3D-  
Printed Material, Cadaveric Specimens, Material Characterization

Copyright © 2023 Anastasia Elizabeth Lucci

## **Abstract**

Material Characterization of Thermoplastic Polyurethane (TPU) and Thermoplastic Elastomers (TPE) for Development of 3D-Printed Surrogate Organs for Medical Training

Anastasia Elizabeth Lucci

Cadaveric specimens are a necessary, albeit limited, resource for training medical students on basic surgical skills. The availability of surrogate 3D-printed organs would readily allow access to resources that could reduce or potentially eliminate the need for cadaveric specimens or, at a minimum, provide students the opportunity to practice with 3D-printed surrogates before transitioning to those specimens. This research focuses on determining which thermoplastic material most closely mimics mechanical properties such as hardness and stiffness of human organs and allows 3D printing surrogate organs to be used as safe, educational tools. Relatively “soft” materials such as thermoplastic polyurethanes (TPU) and thermoplastic elastomers (TPE) are selected as candidate materials for 3D printing of surrogate organs manufactured on a fusion deposition modeling printer (FDM). The mechanical properties of these materials are determined by a series of durometer, tensile, compression, puncture, cutting, and friction tests conducted for different printing configurations and testing conditions. Test results allowed the determination of the most suitable material for manufacturing the 3D-printed surrogate organs. This determination is based on data comparisons to unfixed and fixed cadaveric organs, porcine tissue, or through data reported in the literature. Professional anatomists and pathologists also tested a prototype model manufactured with the selected material to determine the level of realism and practicality of the 3D-printed prototype.

## **Dedication**

Foremost, I am grateful to my parents Christopher and Carrie for always being my biggest fans and encouraging me throughout my academic career. Thank you both for your love and support.

Finally, to my caring, loving, and supportive partner, Andrew, thank you for your patience. I could never have done this without you.

## **Acknowledgements**

I would like to express my sincere gratitude to my research supervisor, Dr. Eduardo M. Sosa, for the opportunity, guidance, and technical advice throughout my study period.

I am also indebted to Bruce Palmer and Sterling Sin of the West Virginia University (WVU) School of Medicine, Department of Pathology, Anatomy, and Laboratory Medicine, and the WVU Human Gift Registry for their collaboration and project resources.

I also want to thank the staff of the WVU Mechanical and Aerospace Engineering Department and my committee members Dr. Gregory Thompson and Dr. Ever Barbero.

Lastly, special thanks to Jordan Friend and the WVU Lane Innovation Hub Staff who patiently took the time to teach me the manufacturing skills necessary to be a good engineer.

# Table of Contents

Abstract.....	ii
Dedication.....	iii
Acknowledgements .....	iv
List of Figures.....	viii
List of Tables .....	xi
<b>Chapter 1. Introduction .....</b>	<b>1</b>
1.1 Background .....	1
1.2 Motivation.....	2
1.3 Objectives.....	3
1.4 Outline .....	4
<b>Chapter 2. Literature Review .....</b>	<b>5</b>
2.1 Introduction.....	5
2.2 A Brief Background on 3D Printing.....	5
2.3 Attempts to Produce Surrogate Organs .....	7
2.4 Material Characterization and Experimental Techniques.....	9
2.5 Safety .....	12
<b>Chapter 3. Materials and Methods.....</b>	<b>14</b>
3.1 Introduction.....	14
3.2 Filaments and Materials.....	14
3.3 Internal Structure of Specimens .....	15
3.4 Experimental Equipment .....	18
3.5 Mechanical Characterization Tests .....	18

3.5.1 Durometer Test.....	19
3.5.2 Raw Filament Tensile Test .....	21
3.5.3 ‘Dog Bone’ Tensile Test.....	22
3.5.4 Unconfined and Confined Compression Test .....	24
3.5.5 Scalpel Puncture Test .....	25
3.5.6 Needle Puncture Test.....	26
3.5.7 Scalpel Cutting Test.....	27
3.5.8 Filament and Glove Friction Testing.....	30
<b>Chapter 4. Results and Discussion.....</b>	<b>31</b>
4.1 Introduction.....	31
4.2 Durometer Testing.....	31
4.2.1 Synthetic Materials .....	31
4.2.2 Cadaveric Organs .....	34
4.3 Raw Filament Tensile Testing .....	34
4.4 ‘Dog bone’ Tensile Testing .....	36
4.5 Unconfined Compression .....	39
4.6 Confined Compression .....	41
4.7 Scalpel Puncture Test .....	43
4.8 Needle Puncture Test.....	47
4.9 Scalpel Cutting Test .....	50
4.10 Friction Test .....	59
<b>Chapter 5. Surrogate Organ 3D-Printing and Cutting Testing .....</b>	<b>61</b>
5.1 Introduction.....	61

5.2 Surrogate Organ Prototype and Survey Design .....	61
5.3 Surrogate Organ Cutting Pilot Test Results.....	63
5.3.1 Methods of Cutting.....	63
<b>Chapter 6. Main Observations and Concluding Remarks .....</b>	<b>68</b>
6.1 Conclusions.....	68
6.2 Study Limitations and Future Work.....	74
<b>8. Appendix A.....</b>	<b>81</b>
<b>9. Appendix B.....</b>	<b>87</b>



## List of Figures

Figure 1. Shore hardness scales with examples (Smooth-On 2023).....	9
Figure 2. How to properly hold a scalpel for a horizontal cut (Kirk, 2002).....	13
Figure 3. Location of infill, walls, and shell in a 3D printed part (BCN3D 2023).....	16
Figure 4. (a) Gyroidal infill 4%. (b) Gyroidal infill 50%. (c) Standard grid infill 4%. ....	16
Figure 5. (a) Rectilinear. (b) Grid. (c) Triangle. (d) Honeycomb. (Cabreira and Santana 2020)..	17
Figure 6. (a) Printed layer orientation diagram (Forster 2015). (b) Printed specimen layer orientation.....	18
Figure 7. Square specimen geometry used for durometer, friction, and scalpel cutting tests. ....	20
Figure 8. (a) Raw filament specimen. (b) Testing fixture with mounted specimen. ....	22
Figure 9. ‘Dog bone’ specimen geometry from standard (ASTM D638-14, 2022) .....	22
Figure 10. (a) ‘Dog Bone’ specimen (slightly bent) using geometry from standard. (b) Printed specimen mounted in tensile testing fixture. ....	23
Figure 11. (a) Cylindrical specimens used for all compression and puncture testing. (b) Mounted specimen for unconfined compression testing. (c) Confined compression fixture with specimen in testing position.....	24
Figure 12. (a) Scalpel puncture test fixture. (b) Needle puncture test. ....	26
Figure 13. (a) 0° with a linear printing pattern. (a) 90° with a linear printing pattern. (c) 90° with an X-hatch. (d) 45° X-hatch. ....	28
Figure 14. (a) Side view. (b) Front view. ....	29
Figure 15. (a) Testing fixture with load cell on right. (b) Specimen can be seen under the black holder.....	30
Figure 16. (a) Hardness measured at the center of the specimen. (b) Hardness measured at the upper lefthand corner of the specimen. (c) Hardness measured at the lower lefthand corner of the specimen. ....	31
Figure 17. Uniaxial raw filament testing results in terms of: (a) Force versus stroke plot (b) Engineering stress versus strain plot. ....	35
Figure 18. Dog-bone tensile test results as function of specimen printing orientation: (a) 0°; (b) 45°; (c) 90°. ....	37
Figure 19. (From left to right) 0°, 45°, 90° print orientation specimens after testing.....	37

Figure 20. Unconfined compression test results as function of infill percentage: (a) 10%; (b) 30%; (c) 50%.	40
Figure 21. Confined compression test results as function of infill percentage: (a) 10%; (b) 30%; (c) 50%.	42
Figure 22. Buckled specimen after confined compression testing.	42
Figure 23. Scalpel puncture test results as function of infill percentage: (a) 10%; (b) 30%; (c) 50%.	44
Figure 24. Scalpel puncture test for all resin materials.	45
Figure 25. Scalpel puncture test results for all porcine organs	46
Figure 26. Scalpel puncture test results for porcine kidney, heart, and muscle tissue.	46
Figure 27. Needle puncture test results as function of infill percentage: (a) 10%; (b) 30%; (c) 50%.	48
Figure 28. Scalpel cutting tests (a) Superficial (1 mm) cut. (b) Deep (6 mm) deep cut.	50
Figure 29. Scalpel cutting test at 1 mm depth of cut results as function of infill percentage: (a) 10%; (b) 30%; (c) 50%.	51
Figure 30. Scalpel cutting test at 6 mm depth of cut results as function of infill percentage: (a) 10%; (b) 30%; (c) 50%.	51
Figure 31. Scalpel cutting test results for specimens with 4% infill and 1 mm depth of cut as a function of print layer direction: (a) 0° linear orientation (b) 90° linear orientation (c) 90° X-hatch orientation (d) 45° X-hatch orientation.	53
Figure 32. Scalpel cutting test results for specimens with 4% infill and 6 mm depth of cut as a function of print layer direction: (a) 0° linear orientation (b) 90° linear orientation (c) 90° X-hatch orientation (d) 45° X-hatch orientation.	54
Figure 33. Scalpel cutting test with (a) perpendicular lines to the direction of the cut. (b) parallel lines to the direction of the cut.	55
Figure 34. Scalpel cross cutting parallel print layers of the specimen.	56
Figure 35. (a) Scalpel cutting test at 1 mm deep for resins with #22 blade; (b) Scalpel cutting test at 1 mm deep for all synthetic materials including TPUs, TPEs, and resins with #11 blade.	57
Figure 36. Scalpel cutting test at approximately 4 mm deep for porcine organs and tissues.	58

Figure 37. (a) Parallel 3D print orientation relative to pulling direction. (b) Perpendicular 3D print orientation relative to pulling direction.....	59
Figure 38. (a) STL file of tonsil model [from JoePKrcma on Thingiverse.com]. (b) Model in 3D printing software with tumor located inside. ....	61
Figure 39. Method of cutting model with the belly of the blade and cutting into small slices. ....	64
Figure 40. Method of cutting model with 45 ° cut.....	64
Figure 41. Method of cutting model with the belly of the blade, making longitudinal and transverse cuts.....	65
Figure 42. R3D-95A Technical data sheet (Raise3D, ‘Raise3D Premium TPU-95A Technical Data Sheet’, June 2021).....	81
Figure 43. PFLX-95A Technical data sheet (Polymaker, ‘PolyFlex TPU95A Technical Data Sheet’, November 2018).....	82
Figure 44. NFLX-85A Technical data sheet (NinjaTek, ‘NinjaFlex 3D Printing Filament’, April 2016) .....	83
Figure 45. NFLX-83A Technical data sheet sheet (NinjaTek, ‘NinjaFlex Edge 3D Printing Filament’, March 2020).....	84
Figure 46. RFLX-82A Technical data sheet sheet (FilaFlex, ‘Recreus Technical Data Sheet, March 2018) .....	85
Figure 47. NTEK-75A Technical data sheet sheet (NinjaTek, ‘Chinchilla 3D Printing Filament’, March 2021) .....	86
Figure 48. Surrogate organ cutting pilot test .....	87

## List of Tables

Table 1. Technical data for each tested material provided by the manufacturer. ....	15
Table 2. Reorganized specimen dimensions from standard (ASTM D638-14, 2022).....	23
Table 3. Durometer test results for TPU and TPE materials. ....	32
Table 4. Durometer test results for resin material.....	33
Table 5. O scale durometer test results for cadaveric specimens. ....	34
Table 6. Maximum stress values at respective elongation percentage.....	35
Table 7. Maximum stress values at percentage elongation at break.....	38
Table 8. Maximum stress values at respective elongation percentage for unfixed organs. (Snedeker et al. 2005).....	39
Table 9. Stress and strain values for unconfined compression testing.....	41
Table 10. Stress and strain values for confined compression testing.....	43
Table 11. Scalpel puncture test force required to puncture outer wall.....	44
Table 12. Scalpel puncture test results for porcine tissues and organs. ....	47
Table 13. Needle puncture test force values for all infill percentages. ....	48
Table 14. Manual Insertions, reformatted from Maurin et al. 2004. ....	49
Table 15. Robotic Insertions, reformatted from Maurin et al. 2004. ....	49
Table 16. Superficial and deep scalpel cutting depths with average forces by infill percentages and material types. ....	52
Table 17. Scalpel cutting depth (1mm) with average forces with 4% infill as a function of print layer directions.....	54
Table 18. Scalpel cutting depth (6mm) with average forces with 4% infill as a function of print layer directions.....	54
Table 19. Perpendicular and parallel cut direction average force values.....	56
Table 20. Average cutting forces for resin materials using #22 and #11 blades. ....	57
Table 21. Parallel 3D print orientation data table for friction testing. ....	60
Table 22. Perpendicular 3D print orientation data table for friction testing.....	60
Table 23. Summed ease of cutability scores for each infill assigned by participant. ....	66
Table 24. Assigned scores by participants for each statement. ....	66

# **Chapter 1. Introduction**

## **1.1 Background**

Medical students at the early stages of their education heavily rely on the dissection of cadavers to learn surgical techniques and clinical anatomy. Cadaveric organs are currently the only realistic hands-on learning tools available to West Virginia University (WVU) allied health students and students worldwide, and hospitals and medical facilities are facing a scarcity of cadaveric organs (Singh et al., 2021). Medical students often gather into relatively large groups, taking turns observing and practicing with a single cadaveric organ or specimen. As a result, these students receive limited exposure to surgical and dissection techniques due to availability. Furthermore, preserved cadaveric organs may not exhibit the same mechanical properties as fresh tissue anatomy.

A commonly used alternative to cadaveric organs is porcine tissues harvested from various commercial food-grade sources. Previous studies indicated that, “in almost every case, fetal pigs have the same muscles as humans, with some small variations in the size and location of some muscles related to the fact that pigs are quadrupedal, and humans are bipedal” (Human/Pig Comparisons, 2004). While these tissues have the most comparable material properties among accessible animals, porcine surrogates do not necessarily match human anatomy (e.g. pig livers possesses five lobes while humans only have four), resulting in a less accurate learning model (Human/Pig Comparisons, 2004).

Clearly, an alternative clinical training tool that addresses the shortcomings of cadaveric organs and porcine models would provide a useful resource in medical training, and three-

dimensional (3D) printing of synthetic surrogate organs for medical training purposes may address the problems of both approaches. The medical field has adopted 3D printing technology, creating many new developments in healthcare training and treatments. This additive manufacturing method allows the creation of accurate anatomical models at a relatively low cost; 3D printed prototypes have allowed planning of surgeries, patient education, creation of prosthetics, and cost-effective student training (Su & Al’Aref, 2018). These printed prototypes can also be customized to create organ models that include abnormal features such as tumors in gallstones, kidney stones, and tonsils placed strategically inside these synthetic specimens. This model customization allows students to search for these abnormalities and better understand how diseases can appear in the body. In combination with computer-aided design (CAD) software, 3D printing offers a broad range of possibilities for creating synthetic organ specimens for medical training.

## **1.2 Motivation**

Human organs used for training medical students are often preserved with embalming fluid which “fixes” tissues to prevent further deterioration. However, this process also causes the organs to harden with respect to fresh or ‘unfixed’ organs (Gerostamoulos and Schumann, 2023), making the specimens potentially unsafe to cut with a scalpel, and rendering preserved cadaveric organs less suitable for learning and training purposes. Thus, the final chosen material for a surrogate must behave similarly to a fresh organ, while also deemed ‘safe’ to cut with typical surgical tools.

To solve the issue present with preserved organs, multiple experimental applications are being tested using flexible 3D printable materials (Garcia et al. 2018). The ability to create

accurate anatomical models at a relatively low-cost using 3D-printed prototypes allows the planning of surgeries, patient education, prosthetics creation, and cost-effective training. Despite these advantages and applications, there is a need for more of this research into the mechanical characteristics of flexible 3D printable materials for use in the medical field. This study initially aims to benefit WVU medical students and staff by providing accessibility to this anatomical education technology. It is expected that the results obtained in this research can be generalized for broader implementation.

This work aims to address economic concerns and feasibility by using FDM technology with selected TPU/TPEs. While more advanced technology is present and up and coming, this advanced technology can be costly. The goal is to fabricate an affordable synthetic surrogate organ with an estimated cost per unit between ~\$1 to ~\$10 depending on the size of the organ.

### **1.3 Objectives**

The main objective of this research is to identify suitable 3D printable material and structures that can be used to create low-cost 3D printable surrogate organs for medical training that closely models a fresh human organ. The model must be safe to cut with a scalpel, meaning that the material/infill must be soft enough that the material can be cut through easily without excessive force. Safety is the most crucial factor of this model; if the model cannot be realistic and safe concurrently, then safety is prioritized. Various materials will be tested to characterize their mechanical properties and compare them to human or porcine organs to assess their level of similarity. This work also aims to compare the data findings with the experience of anatomists from WVU School of Medicine to evaluate levels of similarity between surrogate organs and fresh organs. The specific objectives of this work include:

- Identify and select materials and infill percentages that are accessible and 3D printable to potentially mimic organ material.
- Conduct mechanical characterization test of selected materials for different loading, infill percentages, and print layer orientations.
- Compare experimental data to fixed and unfixed organs or tissues to determine similarities with 3D printed materials.
- Conduct a survey with anatomists determining their opinions on the overall final surrogate organ, material, and infill percentage.

## **1.4 Outline**

This document is divided into six chapters. Chapter 1 presents background information and context for the proposed research along with the main objectives of this work. Chapter 2 presents a literature review of previous research as well as an overview of mechanical characterization tests typically used for thermoplastic materials. Chapter 3 describes materials and methods implemented for characterization tests, including testing fixtures used, the geometry of each specimen, and the types of data each test will provide. Chapter 3 also presents the types of filaments selected for testing as well as selected internal 3D print structures. Chapter 4 provides the results of each test comparing to data collected from similar research on human and/or porcine organs. Chapter 5 discusses the pilot scalpel cutting test conducted with anatomists and the results of the survey taken concluding the trial. Chapter 6 presents the conclusions from this research and includes future recommendations for further research.



## **Chapter 2. Literature Review**

### **2.1 Introduction**

This chapter presents an overview of current 3D printing methods and their use in medical applications. The experimental techniques needed to test materials are evaluated and compared to current standards.

### **2.2 A Brief Background on 3D Printing**

Additive manufacturing, or 3D printing, has existed for over 30 years. Innovative due to its cost-effectiveness and reduction in labor as compared to traditional manufacturing methods, 3D printing of mechanical structures has become a common solution to difficult engineering and manufacturing problems. Particularly, the ability to print 3D objects which incorporate fine structures within the component provides unique abilities previously not available using more conventional fabrication techniques. These abilities of 3D printing are well suited to the current problem of manufacturing surrogate training organs. Fusion Deposition Modeling (FDM), the most common method of 3D printing, works by feeding a filament of material into a heated extruder which melts and deposits the material in a thin layer on the build platform. As this process repeats, subsequent layers are accurately positioned and bond together forming the finished 3D product (Horvath, 2014). Thermoplastic Polyurethanes (TPU) and Thermoplastic Elastomers (TPE) are soft 3D printing materials which are able to be manufactured on an FDM printer. While these materials have extremely similar qualities, TPU has a smoother finish than TPE, which possesses a more rubber-like finish (Xometry, 2022). Both materials have the potential to produce realistic representations of human tissues for the creation of synthetic and realistic human organs.

At its early stages, the 3D printing process was revolutionary to rapid prototyping, allowing a faster and more cost-effective method to test a product or part before mass production. Since its inception, the process has evolved and modern 3D printers allow precise manufacturing with a multitude of materials. 3D printing is the process of creating a three-dimensional object from a digital file, allowing the creation of complex shapes and designs potentially unable to be made using traditional manufacturing methods. FDM prints often have an outer wall or ‘shell’ with an internal structure filled with a specified volumetric density, referred to as infill. Different mechanical tests are needed to assess the outer wall and the internal structure to later create the most realistic representation of an organ. The stacked layers from FDM printing can cause the side surfaces of the print to become rougher than the top or bottom layer (Buj-Corral, et al., 2019). The surface roughness of a material directly relates to the coefficient of friction and influences how well the part can be held by hand or cut by a scalpel. Therefore, print orientation is important in determining the friction against other materials.

In addition to the TPU and TPE materials tested, a group of potentially flexible resins were tested as well. Stereolithography (SLA) printing, or resin 3D printing, has many advantages including increased print resolution, the ability to print softer materials, tighter tolerances, and smoother surfaces (Formlabs, 2023). There are other materials and methods used in 3D printing, although can be more expensive and difficult to print. Silicone 3D printing is a new material available and is unique for its great softness (up to 20A) compared to other 3D printable materials, although it is much more difficult to print accurately because of its high viscosity (3Dprinting.com, 2023).

## 2.3 Attempts to Produce Surrogate Organs

Research conducted by Radenkovic (2016) attempted to develop functional hollow human organs with low anatomical architectural complexity. This research was developed in effort to create organs for transplants due to lack of donors and included development of arteries, trachea, larynx, and facial reconstruction of ears and nose via 3D cell-printing. This process, also known as 3D bioprinting, involves construction of anatomically and physiologically correct tissues through precise modeling and layering of various cellular compositions. The challenges faced by this research were twofold: making the cost sufficiently low enough for patient accessibility, and fabricating organs in a timely manner. Biologically printing cells costs roughly \$280,000 to \$300,000 per organ to produce, which can be cost-prohibitive for the average patient (Radenkovic, et al., 2016). In the United States, an average of 20 people die every day waiting for an organ transplant (Brownell, 2019).

Chu (2023) created a 3D printed synthetic patient-specific soft heart model used to help inform proper stent sizing in surgeries to correct aortic stenosis, a condition which is caused by narrowing of the aortic valve which prevents blood flow. This condition is often corrected by widening this valve with a stent surgically inserted into the patient. However, sizing the stent before surgery is difficult. Researchers scanned the patient's heart and then converted the scan into a 3D CAD model which was 3D printed using a soft, flexible material to create a shell in the shape of the patient's heart. This 3D model was internally mechanized and used to measure blood flow in vitro with different stent sizes to determine the correct size of the implant by simulating pumping actions of the robotic heart and monitoring vitals to determine the best size fit for the patient. While this technology is not able to be implanted, it is a groundbreaking way

to prepare for surgery. Additionally, these heart models may open doors for testing new therapies for heart disease (Chu, 2023).

In 2016, Tan (2016) developed an anatomically accurate patient-specific acrylic cranioplasty implant by using a low-cost commercial 3D printer. Cranioplasty, the surgical repair of the skull, is typically done manually by sculpting putty to fit the missing bone and must be completed within the time it takes the putty to dry, often leading to less than satisfactory results. This study determined that it is feasible to 3D print these implants using models obtained through high resolution CT scans. The ability to 3D print patient-specific prosthetics and implants creates a promising future for personalized, low-cost, medicine. Research in developing these techniques and technologies can develop new solutions to illnesses and existing surgical procedure limitations (Tan, Ling, and Dinesh 2016).

Similarly, a smart prosthetic ear was fabricated using a polymeric ‘smart material,’ Polyvinylidene Fluoride (PVDF). This was done by using PVDF, which exhibits favorable piezoelectric, pyroelectric, photo-pyroelectric and ferroelectric response properties, as a sensor or transducer. This material was able to generate electric potentials proportional to pressure and temperature changes. The prosthesis was able to provide proportionate electrical stimulus to the skin via the nervous system. A prosthetic that allows for sensory perception could potentially create a new world of prosthetic devices for patients (Suaste-Gómez et al. 2016).

This literature is meant to explain existing attempts to 3D print models or implants, by using different methods or materials. While some of these applications are patient specific, others are an attempt to develop training techniques and pre-surgery planning. Some of this work also faces the challenges of affordable costs, and availability.

## 2.4 Material Characterization and Experimental Techniques

Manufacturers of 3D printable soft materials specify values of Shore hardness to provide an indication of the level of hardness of their products. Shore hardness is a family of scales used for measuring the hardness for a range of soft and plastic materials. Figure 1 shows the three typical scales used for a variety of different common materials. Each scale ranges from 0 to 100, with zero being the softest and 100 being the hardest. These scales slightly overlap, for example a material with a Shore hardness of 95A would be comparable to a Shore ~50D hardness. The OO scale is often used to quantify the hardness of very soft gels and some soft rubber materials. The A scale measures the hardness of flexible rubber-like materials from very soft to semi rigid plastics. Finally, the D hardness scale measures hard rubbers and plastics.

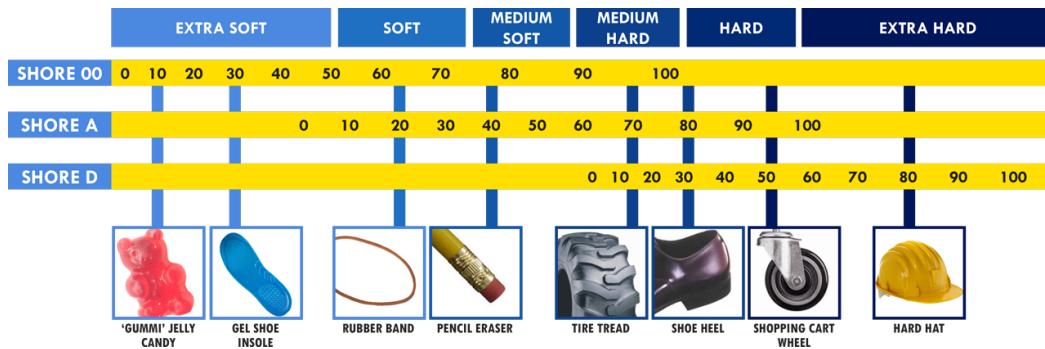


**Figure 1. Shore hardness scales with examples (Smooth-On 2023).**

Unfixed organs are typically on the Shore OO scale in the low to mid-range (Yoon et al. 2017). Material of this softness is virtually impossible to print with the average FDM printer. Silicone printers and other more sophisticated material printing is possible, although much more expensive than a basic FDM printer. This work aims to find solutions that can be materialized with a low level FDM 3D printer which can be accessible to virtually any organization regardless

of expertise or resources. For this type of printer, the closest alternative is to use materials with hardness in the Shore A scale, which is the typical scale for TPU or TPE materials. The hardness of a specific material is often measured using a calibrated handheld durometer to verify values after printing due to potential variations in hardness between spools of filament. A durometer measures resistance to indentation by recording the reaction force of a material via a calibrated spring when it is pressed onto the material (Qi, et al., 2003).

Tensile testing methods are often used to determine uniaxial stretching properties for a variety of plastic materials. Before the 3D printing process, the properties of the material are determined by examining the raw filament. (Oviedo et al. 2020). Tensile testing data provides the candidate material's ductility and strength under uniaxial tensile forces, this will be compared to the manufacturer's specified values for the material. The filament is attached at the top and bottom of a Bollard tensile style grip and the gauge length is measured at 100 mm.

The 'Standard Test Method for Tensile Properties of Plastics' (ASTM D638-14, 2022) specifies a standardized testing bar 'dog bone' geometry with two shoulders that taper to a small center gauge. The testing standard also states that within a given series of specimens care must be taken to secure the maximum degree of uniformity in details of preparation, treatment, and handling (ASTM D638-14, 2022). The material is 3D printed to form this shape to measure the material properties after the 3D printing process. For both types of tests, the machine will elongate the specimen with a defined speed, while recording the force required to pull the specimen apart (Letcher and Waytashek 2014).

Compression testing methods are used to determine the force required to compress material over a specified distance. Elastic stiffness can be defined as the ability of a material to restore to

its original state after subject to given load (Xia, et al., 2017). Compression properties tests are typically determined following the “Standard Test Method for Compressive Properties of Rigid Plastics” where a sample of flexible plastic material is compressed until it fractures or deforms into a flat disk (ASTM D695-15, 2015). Cartilage biomechanics are often analyzed by performing confined and/or unconfined compression tests which are described in more detail in Chapter 3 (Boschetti, et al., 2004).

To ensure that the candidate synthetic materials are easy to hold in the hand with a surgical glove, a friction test is needed. The results of the friction tests are intended to assess how safely medical students can perform cuts while holding the 3D printed specimens in their gloved hand or against a table with their hand. This test is conducted under dry conditions of both materials, as wet conditions result in a reduced friction environment. Care was exercised to ensure that the rate of motion of the equipment was carefully controlled. The standard used for this testing was the “Test Method for Static and Kinetic Coefficients of Friction of Plastic Film and Sheeting” (ASTM D1894 2011). This standard was withdrawn and not replaced after the testing was completed in March of 2023.

‘Incision with precision’ is a scalpel cutting method that positions the blade vertically 90° for the initial puncture into the skin. The blade penetrates through the skin until it reaches a position where no resistance is felt which indicates that the blade has breached completely through the dermis. Then the scalpel is tilted to an angle of 45° using the curved cutting edge to make the incision (Chandra et al. 2018). When evaluating the puncture resistance of a material, the ASTM F1342 standard test (ASTM F1342 2022) is a commonly used material characterization method. This standardized is also frequently used when performing biopsies of soft tissues. According to

the American Journal of Roentgenology, blunt needles are commonly used to navigate in fat and preserve vital structures during a biopsy (De Bazelaire et al. 2009).

A study conducted by Chanthasopeephan, et al., (2006) addressed the specific reaction of soft tissue to a cut with a scalpel blade. This experiment measured the cutting force required as a function of cut length and depth to determine tissue resistance. Pig liver was used as the sample material which is a common replacement for soft-tissue (Ntonas et al. 2020). The combination of this study and Chandra's research served as a basis for fixture design and material cut resistance measurements for porcine tissues and the selected 3D printed materials.

## **2.5 Safety**

While there are no rigid requirements to determine the amount of force that can be safely applied to a scalpel while cutting, it is advised to “never put excessive force on a sharp” (Princeton University Lab Safety Guidelines). If the cutting force is such that the operator can no longer easily control the instrument, the cut is defined as unsafe. The forces required to cut these materials will determine whether each material is realistic and/or safe for student use. In dermatologic surgical techniques the preferred cutting angle is 45° which utilizes the maximum amount of sharpened blade (Chandra et al. 2018).

The textbook “Basic Surgical Techniques” (Kirk, 2022) explains and illustrates common methods of teaching the strategies necessary to carry out common surgical techniques and procedures. The “Instrument Handling” section explains the proper way to hold and operate a scalpel: “Draw the knife blade under controlled pressure to determine the depth of cut.” These instructions help guide students to a better understanding of how to conduct these motions safely.



The text provides additional instructions for holding the scalpel while cutting skin, instructing to “draw the belly of the knife, not the point, across the skin” as shown in Figure 2.

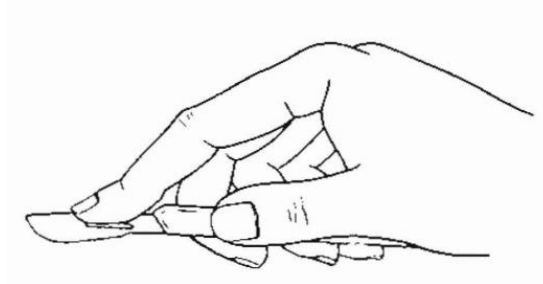


**Figure 2. How to properly hold a scalpel for a horizontal cut (Kirk, 2002).**

Additionally, the text emphasizes the importance of using forceps to safely dispose of a blade to avoid accidental finger laceration in case of slipping (Kirk, 2002). Finally, it is critical to use a sharp scalpel, to keep the cut consistent.

## **Chapter 3. Materials and Methods**

### **3.1 Introduction**

This chapter describes the materials and testing methods implemented for characterization of candidate 3D printed surrogate organ material mechanical properties while describing why each test was crucial for this study. The testing equipment, fixtures, and software used throughout this study are presented with their respective specifications. Details regarding specific testing fixtures and specimen dimensions are explained and justified.

### **3.2 Filaments and Materials**

The candidate materials were chosen based on existing material for the available 3D printing machine (Raise3D, Pro 2, 3D), comparable hardness, and availability from well-known filament companies. The materials are listed along with their identifying shortened name used in the experiments: Raise 3D TPU 95A (RFLX-95), Polyflex TPU 95A (PFLX-95), Ninjaflex TPU 85A (NFLX-85), Ninjaflex TPU 83A (NFLX-83), Recreus Filaflex TPU 82A (RFLX-82), and Ninjatek Chinchilla TPE 75A (NTEK-75). The specimens were printed within the manufacturer's recommended settings compiled in Appendix A . Table 1 shows selected technical data for each material tested in this work. Technical data sheets for each material can be found in Appendix A.

Materials chosen were assessed on the Shore A hardness scale. This measurement denotes material hardness on a scale from 0 to 100, where larger values indicate increased material hardness. To meet the objectives of the work, the material must be “stiff” enough for the surrogate organ to be self-supporting (preventing collapse when surgical pressures are applied), while still being soft enough to mimic the organ hardness.

**Table 1. Technical data for each tested material provided by the manufacturer.**

Material ID	Density (g/cm <sup>3</sup> )	Hardness (Shore)	Tensile Strength (MPa)	Melting Point (°C)	Elongation at Break (%)
R3D-95A	1.20-1.24	95A	29.0±2.8	210	330±15
PFLX-95A	1.20-1.24	95A	29.0±2.8	210	330.1±14.9
NFLX-85A	---	85A	26	216	660
NFLX-83A	---	83A	25	180	900
RFLX-82A	1.12	82A	45	215	650
NTEK-75A	---	75A	22	180	600

The three resins used were White 39A, Elastic 50A, and Flexible 80A. These materials were chosen because their specified hardness is lower or equivalent to the TPU and TPE materials. The Elastic 50A and Flexible 80A resins are both produced by Formlabs (Somerville, MA, USA) and were printed on a 3B+ resin printer using Preform software. The White 39A is produced by Resione (Dongguan Godsaid Technology Co., Ltd. Dongguan, China), and printed on an Anycubic (Shenzhen, China) Photon M3 Premium resin printer using Lychee (Mango3D Mérignac, France) software. All specimens were printed solid, as Preform does not include any infill features. The experiments conducted with the resin were the durometer test, scalpel puncture test, and the scalpel cutting test (1 mm deep). Technical data sheets for each material can be found in Appendix A

### **3.3 Internal Structure of Specimens**

As mentioned in Chapter 2, the name for the internal structure of each 3D printed part is called ‘infill’ and can be selected from many different geometries and densities available in the specific slicing software used. The image seen in Figure 3 illustrates the location of the infill (yellow), walls (green), and outer wall or shell (red) in a 3D printed part.

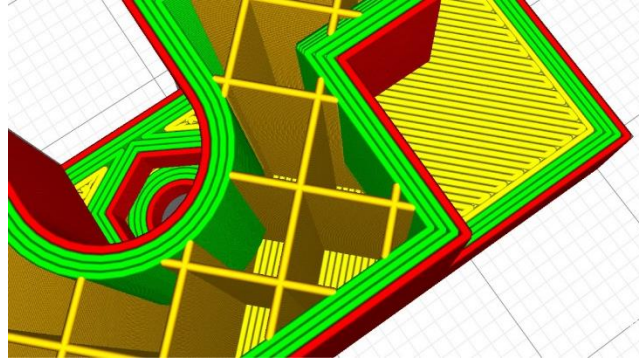


**Figure 3. Location of infill, walls, and shell in a 3D printed part (BCN3D 2023).**

The slicing software used for digital preparation of specimens was ideaMaker (Raise3D, Irvine, CA, USA), version 4.2.3, which generated the G-code used to numerically control the 3D printer. The infill chosen across all FDM specimens (unless specified otherwise) in this study is classified as ‘gyroidal’ infill. A gyroidal infill is a 3D geometry often used to create porous structures. One beneficial characteristic of the gyroidal infill, as opposed to grid, triangular, and hexagonal, is the gyroidal fill’s near isotropic force response regardless of load orientation. The advantage of this infill pattern is that only the orientation of the outer wall with respect to the cutting blade must be considered. Specimens created using gyroidal infills allow flexibility in placement and orientation during testing. Examples of infill types and densities used in this research can be seen in Figure 4, while other common infills are shown in Figure 5.

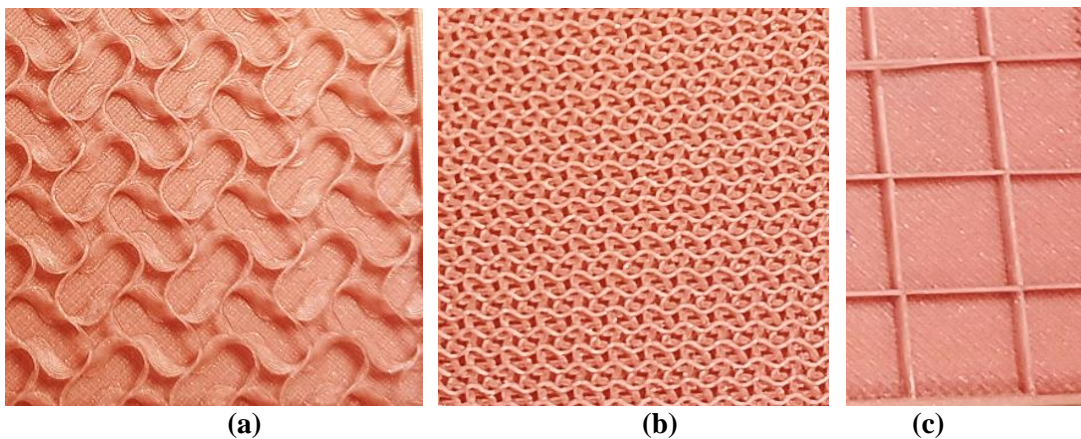


**Figure 4. (a) Gyroidal infill 4%. (b) Gyroidal infill 50%. (c) Standard grid infill 4%.**

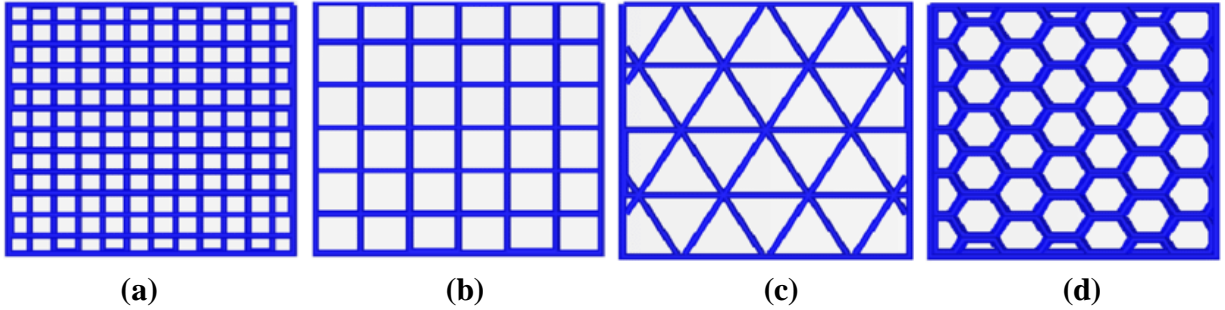


**Figure 5. (a) Rectilinear. (b) Grid. (c) Triangle. (d) Honeycomb. (Cabreira and Santana 2020)**

Gyroidal patterns are naturally occurring and can be found in the wings of butterflies (Wilts et al. 2017). The equation for gyroidal infill is a function of the position in space, where  $x$ ,  $y$  and  $z$  correspond to each dimension and can be seen in Eq. 1.

$$\cos(x)*\sin(y) + \cos(y)*\sin(z) + \cos(z)*\sin(x) = 0 \quad \text{Eq. 1}$$

The required cutting force of the materials is correlated to material density. As organs vary in density, their cutting forces will not be consistent across different types of organs because of their unique makeup of muscle, tissue, and other factors (Annexes A-D 2009) requiring the evaluation of several infill percentages. A higher internal volumetric density directly corresponds to a higher infill percentage. A specimen with a 100% infill would be filled solid, while a 0% infill means the specimen has an outer shell and an empty internal space. The densities chosen for this research were 4%, 10%, 30% and 50%. Densities greater than 50% required excessive cutting forces and therefore were excluded for safety reasons. The wall thickness of 1mm was chosen to match the cutting-edge height of the scalpel blade.

Several of the tests conducted required the printed specimens to contain one of three different “orientations” of printed layers:  $0^\circ$ ,  $45^\circ$ , and  $90^\circ$ . A diagram of the three orientations and the printed specimens used are seen in Figure 6. The  $0^\circ$  orientation corresponds to the print lines of

a specimen that are perpendicular to the ground when mounted vertically into the testing machine.

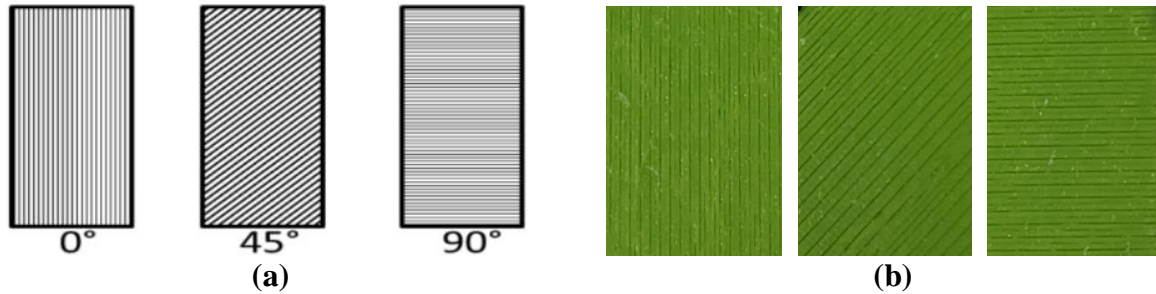


**Figure 6. (a) Printed layer orientation diagram (Forster 2015). (b) Printed specimen layer orientation.**

### **3.4 Experimental Equipment**

The testing machine used for all tests, excluding friction test and durometer test, was a compact table-top universal testing machine (EZ-LX, Shimadzu Corp, Kyoto, Japan). The machine is equipped with high precision interchangeable load cells of 500 N and 2 kN capacities accurate to  $\pm 0.1\%$  of the maximum indicated force value. Forces and displacements are measured and recorded using the machine's program: TrapeziumX. A separate 5-kN load cell (RSB3-500M, LoadStar Sensors, Fremont, California) was used for friction testing to ease measurement fixture design requirements. This load cell is accurate to  $\pm 0.1\%$  to  $\pm 0.5\%$  of the 5-kN full scale range.

### **3.5 Mechanical Characterization Tests**

Mechanical testing was conducted to determine the similarity between cadaveric organs and candidate flexible materials. These tests comprise standard characterization tests and custom-

made tests to reproduce specific motions utilized in medical training. Standard tests included hardness test, raw filament tensile test, ‘dog bone’ specimen tensile test, unconfined compression test, and confined compression test. Custom tests included needle and scalpel puncture tests, friction tests, and finally, a scalpel cutting test. The hardness test, raw filament tensile test, and friction test will evaluate “intrinsic” material properties, while the remaining tests will evaluate the 3D-printed simple structures manufactured from the candidate TPU/TPE materials. The following sections provide specific details for each test.

After acquisition, all data was analyzed, and the testing results of this research were then compared to data gathered from similar testing methods on soft tissues and organs reported in the literature. For the multitude of tests conducted in this research, the results are in good agreement with the data obtained from literature and collected from human organs. However, in some instances the data collected in this work is compared to different types of organs due to lack of literature on this subject. Since all tissues are unique, it is difficult to test these tissues and obtain consistent results. Standards used for this work are not directly applicable to 3D printing or fresh tissues, therefore these standards could only be followed as closely as possible.

### **3.5.1 Durometer Test**

Each filament selected for this research was specified to have a hardness measured on the Shore A scale, this was selected for its inherent flexibility and low cost. Specimens for this test were printed as a 50×50×6 mm square with 100% infill as shown in Figure 7. A 100% infill was selected to assess the material hardness by eliminating any error introduced from any internal structures or air trapped within. Each specimen was measured with an Intercomp durometer

(Intercomp, Medina, MN) following ASTM D2240-15 to determine the hardness of each printed specimen. A minimum thickness of 6 mm was required to accurately test the hardness (Prodex Profiles Elastomers). Five measurements in various locations were taken on each side of the solid specimen, all 10 values were averaged to obtain the final experimental hardness of each material. Finally, even though the number of data points was limited, a simplified statistical analysis was performed to determine the standard deviation of the data collected.

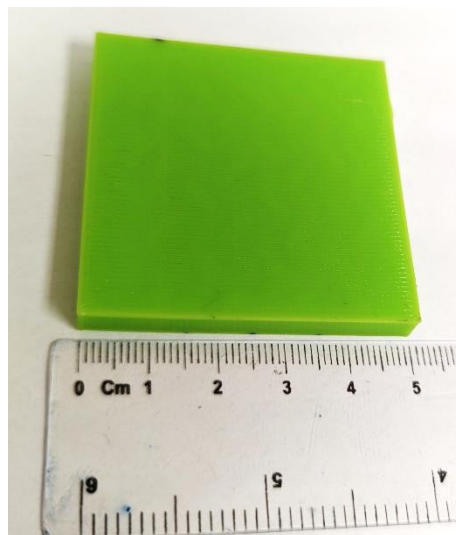


**Figure 7. Square specimen geometry used for durometer, friction, and scalpel cutting tests.**

To better understand the hardness of human organs, a set of hardness tests were conducted on preserved (also called ‘fixed’) and unfixed cadaveric specimens. Access to these specimens was possible through a collaboration with the WVU Department of Pathology, Anatomy, and Laboratory Medicine in addition to the WVU Human Gift Registry. A total of eleven fixed male and female cadavers were tested (aged 58 to 100), and eight unfixed male and female cadavers (aged 57-95 ranging from 4 hours to 120 hours since death) were also tested. Fixed hardness measurements were conducted at multiple body locations and organs, including the forehead,



temple, chin, heart, lung, and liver. Unfixed hardness measurements were restricted to the forehead, temple, and chin. Anatomically, the forehead reading was taken at the center, roughly a half inch above the eyebrow line. The temple reading was taken from the left side, and chin values were taken from approximately one inch below the bottom lip in the center. The fixed surface hardness of the organs was measured at the posterior left ventricle of the heart, the superior portion of the left lung, and the anterior part of the right lobe of the liver.

### **3.5.2 Raw Filament Tensile Test**

This test was conducted to determine tensile strength and elongation at break of each candidate filament strand before 3D printing, as the printing process has the potential to alter the chemical and mechanical properties after undergoing heating, extrusion, and cooling. This data will later be compared to the properties of the material given by the manufacturers' technical data sheet. TPU and TPE materials can be characterized as hyperelastic materials. Hyperelastic materials have a nonlinear stress-strain behavior, and respond elastically when undergoing large deformations, meaning they return to their original shape when the load is removed.

The test specimens comprised at least three 300 mm strands cut from raw filament spools of 1.75 mm diameter. The requisite 300 mm ensures adequate gripping length in a custom-made bollard testing fixture. Due to the large maximum elongation of the material and the maximum displacement of the machine, a 100 mm gauge length was required. Both filament and fixture can be seen in Figure 8(a) and (b), respectively. A machine crosshead speed of 50 mm/min was chosen for all materials as the maximum speed which allowed the material time to adapt and reconfigure during stretch (Letcher and Waytashek 2014). To avoid stress concentration and failure at the gripping points, the raw filament was fed through and looped around a cylindrical

grooved fixed pulley to prevent material slip during testing. The fixture bottom (not shown) and top were identical, and a clamping plate was tightened to further secure the specimen.

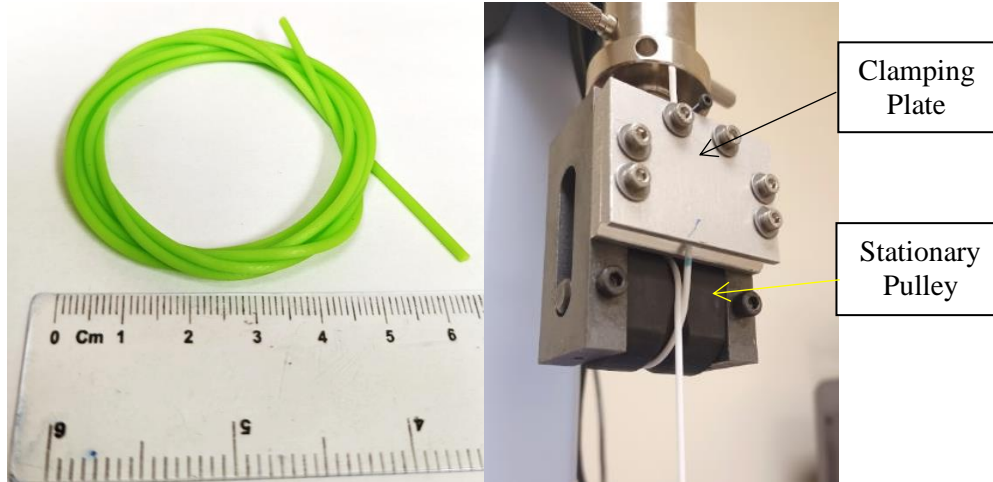


**Figure 8. (a) Raw filament specimen. (b) Testing fixture with mounted specimen.**

### 3.5.3 ‘Dog Bone’ Tensile Test

Tensile testing following ASTM D638-14 was conducted using “dog bone” shaped specimens 3D printed with 100% infill to determine the best print layer orientation with respect to pulling direction. The shape and dimensions of the type V specimens were extracted from the ASTM D638-14, using geometry and dimensions presented in Figure 9 and Table 2, respectively.

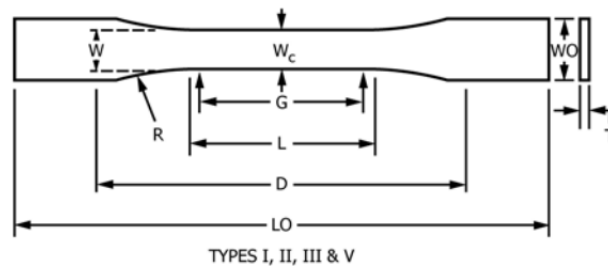


**Figure 9. ‘Dog bone’ specimen geometry from standard (ASTM D638-14, 2022)**

**Table 2. Reorganized specimen dimensions from standard (ASTM D638-14, 2022)**

Dimensions of specimen Type V	[mm]	[in]
W–Width of narrow section	3.18	0.125
L–Length of narrow section	9.53	0.375
WO–Width overall, min	9.53	0.375
LO–Length overall, min	63.5	2.5
G–Gauge Length	7.62	0.3
D–Distance between grips	25.4	1.0
R–Radius of fillet	12.7	0.5
T–Thickness	3.2	0.126

The printed specimens were organized in three groups according to external layer orientations, namely  $0^\circ$ ,  $45^\circ$ , and  $90^\circ$ . Figure 10 shows the holding fixture used during tensile testing with a representative sample specimen in place for illustration purposes. A constant 10 mm/min speed was used for all units evaluated until the material failed or delamination between layers occurred. Tests were conducted with five specimens of the three printing orientations, totaling 15 specimens per material type. The results were averaged, and a simplified statistical analysis was performed to determine standard deviation.

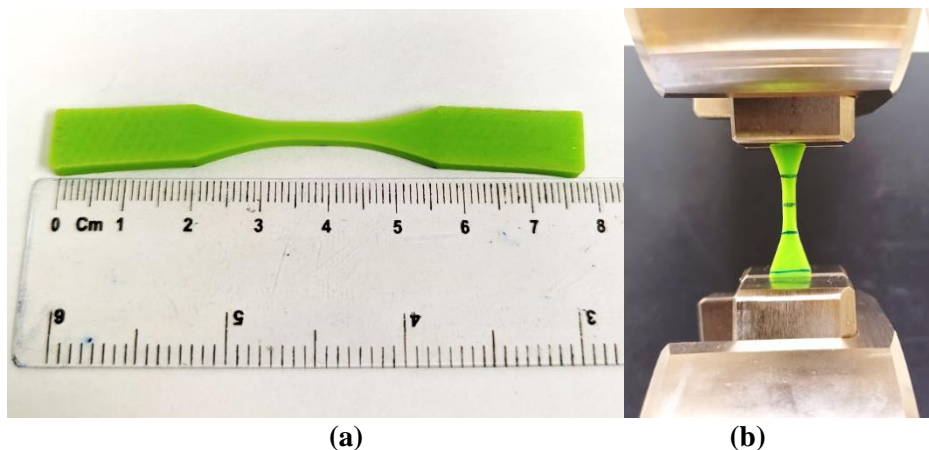


**Figure 10. (a) ‘Dog Bone’ specimen (slightly bent) using geometry from standard. (b) Printed specimen mounted in tensile testing fixture.**

### 3.5.4 Unconfined and Confined Compression Test

Both unconfined and confined compression testing are commonly used for biological tissue evaluation. (Boschetti, et al. 2004). This test determines the stiffness under compressive loads (unconfined and confined) of both the internal structure and the candidate material by comparing the varying infills within the same material and comparing a singular infill among different materials. The maximum force at the material cross section was used to calculate the average stress while the deformation was determined by stroke length. Cylindrical specimens 10 mm in height by 20 mm in diameter were used for all compression testing. This cylindrical specimen geometry was designed to fit the testing fixture of the confined compression test. The rotational orientation of the cylinder is insignificant due to the isotropic-like response to force provided by the gyroidal infills used. Three specimens of each infill density, 10%, 30% and 50% were tested, totaling 9 specimens per material type. The testing speed was set at 1 mm/min to comply with the  $1.3 \pm 0.3$  mm/min range specified in ASTM D695-15 “Standard Test Method for Compressive Properties of Rigid Plastics” and the maximum stroke was 6 mm.

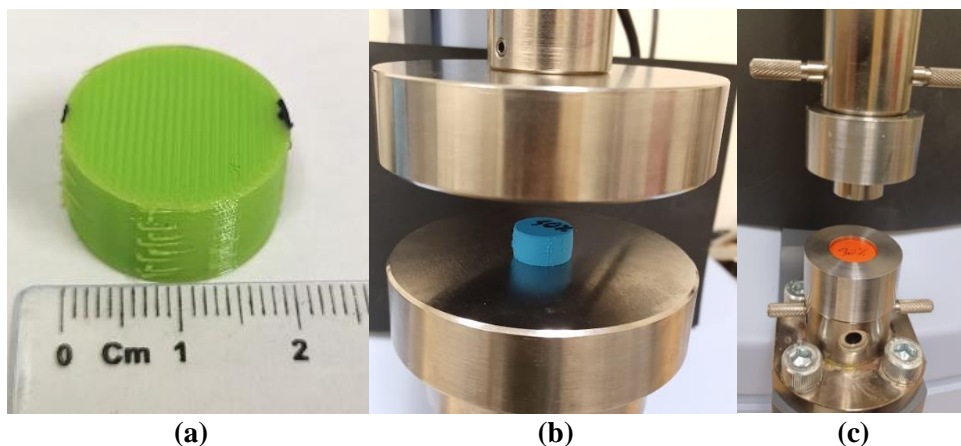


**Figure 11. (a) Cylindrical specimens used for all compression and puncture testing. (b) Mounted specimen for unconfined compression testing. (c) Confined compression fixture with specimen in testing position.**

### 3.5.5 Scalpel Puncture Test

The scalpel puncture tests were conducted to determine the force required to pierce the outer wall of the 3D printed part. A typical procedure for surgical cutting (Chandra et al. 2018) consists of piercing the surface with a scalpel positioned normal to the surface of the desired cut location, followed by tilting the scalpel approximately 45 degrees from the surface and then proceeding with the cut. The scalpel puncture test was designed to measure the force required to pierce the material in the normal position, the 45-degree cutting resistance was measured via the scalpel cutting test described below.

The specimens used for this test had the same geometry as the specimens used for compression testing Figure 11(a) with the same gyroidal infills densities of 10%, 30% and 50%. The test fixture used for this experiment was a combination of a wedge grip holding the scalpel handle, mounted in vertical position with the blade pointing down, and the bottom circular compression plate holding the specimen, as shown in Figure 12. The wedge grip was secured to hold the scalpel in place while the blade punctured the specimen from above. The testing speed was set at 10 mm/min with a maximum stroke of 7 mm. Three specimens of the three infills were tested and averaged, totaling 9 specimens per material type. A new scalpel blade was used for each new material type to minimize cumulative effects associated with increased blade use. The number of punctures performed before replacing the blade was based on research with the effects of blades after multiple cuts (Spagnoli et al. 2019). The surgical blades used throughout these experiments were Havel's Sterile Stainless Steel #22 (Norwalk, CA, USA). Porcine tissue was also tested with this method for comparison with the synthetic material data. The organs tested were as follows: skin (two types), kidney, heart (the apex, right and left ventricles), and muscle

tissue (both parallel and perpendicular fiber orientation to the blade). All skin tested contained the same naturally occurring order of layers: epidermis, dermis, and hypodermis. The samples were inverted to obtain two different testing specimens. The “front of skin” testing first punctured the epidermis, and the “back of skin” testing first punctured the hypodermis. The kidney was cut into  $\sim 10 \times 10 \times 10$  mm cubes containing the renal cortex and renal medulla.

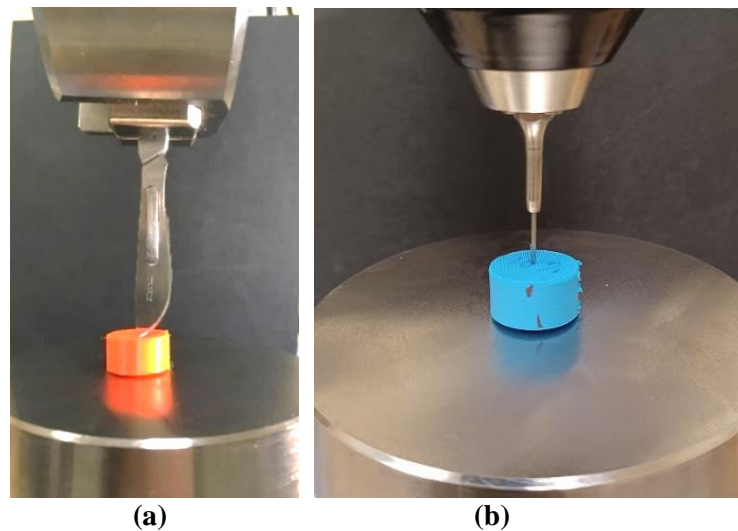


**Figure 12. (a) Scalpel puncture test fixture. (b) Needle puncture test.**

### **3.5.6 Needle Puncture Test**

The needle puncture test was conducted to obtain comparison data to the scalpel puncture test. The needle puncture test mimics a biopsy, a common biological procedure done to organs. In biopsies, blunt-tip stylets are used to take a tissue sample while protecting important structures and steering through fatty tissue (De Bazelaire, et al. 2009). A 20-gauge ( $\sim 0.908$  mm OD) blunt tip needle was used for the tests. The specimens used for this test had the same geometry as the compression testing specimens and gyroidal infill densities of 10%, 30% and 50%. The testing

speed, stroke, and number of sampled specimens were the same as in the scalpel puncture testing to allow for meaningful comparison.

### **3.5.7 Scalpel Cutting Test**

This test measures the force required to produce a cut with the scalpel positioned at an angle of  $45^\circ$  with respect to the cutting surface. This test was designed to mimic the typical procedure for surgical cutting at  $45^\circ$  (Chandra et al. 2018) as mentioned in section 3.5.5. The force measured for the synthetic materials was then compared to the  $45^\circ$  cutting resistance of porcine organs tested with the same fixture. The scalpel cutting testing was conducted with square specimen geometry identical to those used for hardness testing (Figure 7). In addition to the three previously used infill percentages of 10%, 30%, and 50%, an additional test using 4% infill was conducted to assess the smallest infill, which would retain adequate internal structure and model integrity without collapse. Testing was conducted in a similar manner using both printed materials and porcine tissue. The printed materials were composed of TPU, TPE, and three resins: White 39A, Elastic 50A, and Flexible 80A. Furthermore, two configurations were tested for Resin-White 39A, a 100% infill (solid) specimen (6 mm thick), and a second specimen made from a stack of three slices of 2 mm thick material to model a 6 mm thick specimen. Two cut depths of 1 mm and 6 mm were utilized. The first measured the force to cut the specimen wall only, while the second measured the cutting forces of both the wall and infill together. Four outer layer print orientations were selected for testing: (a)  $0^\circ$  with a linear printing pattern, (b)  $90^\circ$  with a linear printing pattern, (c)  $90^\circ$  with a X-hatch printing pattern, and (d)  $45^\circ$  with a X-hatch printing pattern as shown in Figure 13. The ‘linear’ printing pattern refers to each layer printed in the same direction, where an X-hatch pattern refers to each layer alternating orientation by  $90^\circ$ .

In Figure 13, the blue arrows in the images represent the top layer while the red arrows represent the adjacent layer underneath. These printing patterns were chosen to determine the potential variance in cutting forces as a function of the print orientation in the specimen wall.

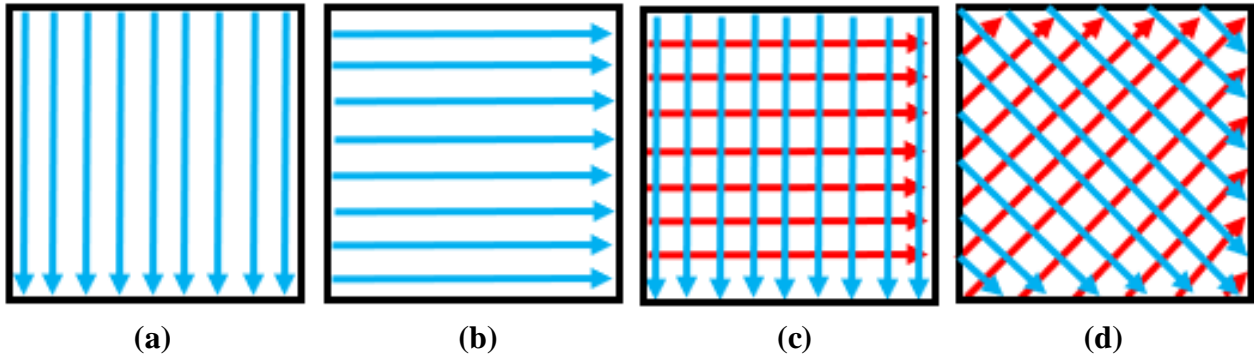


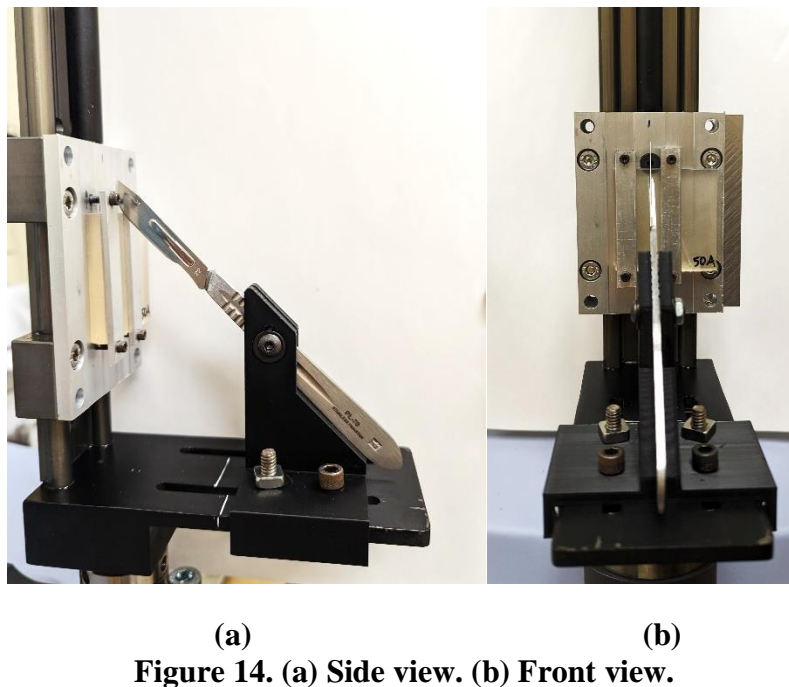
**Figure 13. (a) 0° with a linear printing pattern. (b) 90° with a linear printing pattern. (c) 90° with an X-hatch. (d) 45° X-hatch.**

Tests were conducted on porcine tissue utilized organs (skin (two types), kidney, heart (the apex, right and left ventricles), and muscle tissue (both parallel and perpendicular fiber orientation to the blade). The porcine tissue data was compared to the collected synthetic materials data.

A new test fixture was designed and manufactured specifically to perform the scalpel cutting test. The fixture consists of a stationary scalpel mount and a sliding carriage transporting the specimen attached to the testing machine. The design of this new fixture is based on a similar fixture created by (Chanthasopeephan, Desai, and Lau 2006) to determine the cutting resistance of a pig liver. The machine used in this research utilized a similar testing method, although their setup was created to operate and cut horizontally. In this work, the fixture was designed to cut vertically to ensure its compatibility with the Shimadzu tabletop testing machine. The fixture allowed the testing machine to pull the specimen attached to the carriage upwards, while



recording the force exerted by the scalpel during the vertical cutting of the specimen. The scalpel was mounted onto a standard handle and kept stationary at the desired 45° angle with respect to the base support as shown in Figure 14. The specimen traveled upward at a speed of 25 mm/sec through the scalpel blade. Testing consisted of producing three equidistant cuts (10 mm apart) per specimen. The scalpel blade was replaced after every new specimen to maintain similar cutting conditions for all specimens and reduce the effect of blade dulling. The surgical blades used throughout these experiments were Havel's Sterile Stainless Steel #22 and Bard-Parker Carbon Steel #11 (Van Nuys, CA, USA). In medical applications, #22 blades are primarily used for larger incisions, whereas #11 blades are used mainly for piercing or short incisions (USA Medical and Surgical Supplies, 2018). The carriage and rail were purchased from McMaster-Carr. This new fixture was designed and manufactured by the author with assistance from the WVU Lane Innovation Hub (WVU, 2022).



(a) (b)  
**Figure 14. (a) Side view. (b) Front view.**

### 3.5.8 Filament and Glove Friction Testing

Friction testing was conducted to evaluate the friction between a surgical glove and the 3D printed specimens of the candidate materials. The specimen geometry used for the friction tests is identical to the square specimen shown in Figure 7. A specimen holder was designed and constructed to hold a 1 kg weight on top of the 3D printed specimen, which was seated in a cavity underneath as shown in Figure 15. The specimen holder ensured contact only between the platform and the printed specimen. The platform consisted of a plate with a surgical glove stretched over it and secured with tape ensuring flat contact surface between the 3D printed specimen and the surgical glove. The 1 kg weight acts as a consistent normal force while a horizontal force is applied by pulling the load cell by hand, the weight of the specimen holder was negligible. The specimen holder was pulled 70 mm at a speed of approximately 20 mm/sec to simulate quasi-static conditions. The resulting horizontal pulling force was recorded with the load cell control software (SensorVUE, LoadStar Sensors, CA). Five specimens were tested per material, per orientation. All printed specimens were 100 infill (solid). Perpendicular and parallel print layer directions to the pulling direction were tested. With four materials and two orientations, forty trials were tested in total.

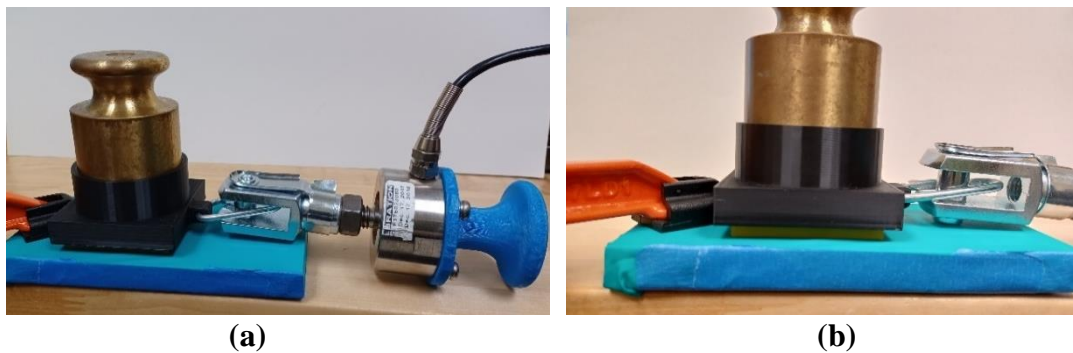


**Figure 15. (a) Testing fixture with load cell on right. (b) Specimen can be seen under the black holder.**

## Chapter 4. Results and Discussion

### 4.1 Introduction

This chapter presents material characterization test results of all materials tested following the methods and procedures outlined in Chapter 3. Synthetic materials are assessed by suitability of use to manufacture surrogate organs and, where appropriate, are compared to organ tissue values found in the literature.

### 4.2 Durometer Testing

#### 4.2.1 Synthetic Materials

Durometer testing was conducted as described in section 3.5.1. Data was acquired and averaged to obtain measurements illustrated in Table 3, listed from hardest to softest based on values supplied by the manufacturer. Differences between experimental values and specified values are expressed as percentages.

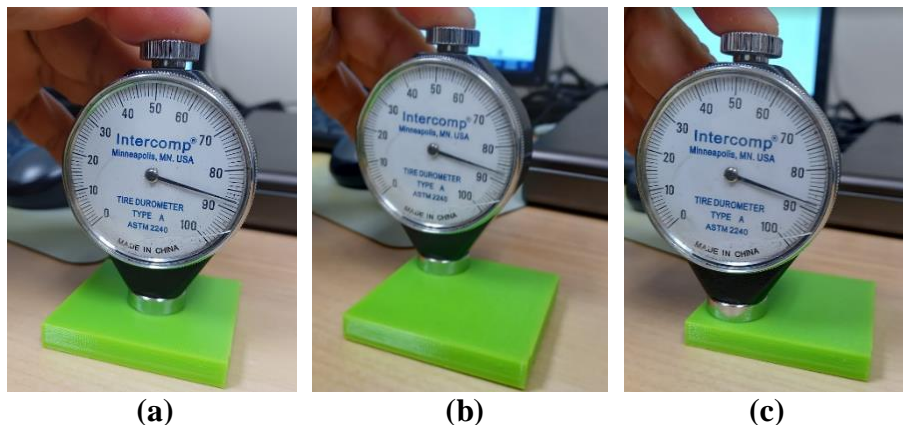


**Figure 16. (a) Hardness measured at the center of the specimen. (b) Hardness measured at the upper lefthand corner of the specimen. (c) Hardness measured at the lower lefthand corner of the specimen.**

**Table 3. Durometer test results for TPU and TPE materials.**

Material ID	Specified [SU]	Measured [SU] (SD)	Percent difference
R3D-95A	95	94.7 (1.5)	-0.3%
PFLX-95A	95	87.1 (4.0)	-8.3%
NFLX-85A	85	84.3 (1.3)	-0.8%
NFLX-83A	83	81.6 (1.5)	-1.7%
RFLX-82A	82	85.5 (1.3)	4.3%
NTEK-75A	75	76.4 (0.7)	1.9%

Notes: SU Shore Units; SD: Standard Deviation

Even though the number of measurements was somewhat limited, experimental results tend to reveal that PFLX-95A is softer than the values specified from the manufacturer by ~8.3%. The manufacturer's specified values determine RFLX-82A to be the second softest material, where the experimental data determines it to be the third hardest material resulting in a (4.3% difference). The materials manufactured by NinjaTek (NFLX-85A, NFLX-83A, NTEK-75A), as well as the material produced by Raise 3D (R3D-95A), held relatively true to the specified values with less than 2% difference. The material with the lowest standard deviation is NTEK-75A and the highest standard deviation is PFLX-95A. The large standard deviation of PFLX-95A is likely due to changes in material properties related to the printing process.

Estermann, et al. (2020) conducted a study to determine the Shore hardness of porcine and bovine liver tissue compared to various 3D printing materials. In their study, they used a Shore OO durometer, which is for softer materials than those in the Shore A scale, where a 40 on the OO scale equates to the starting point (0) on the A scale. Their results showed that the hardness of a porcine liver was approximately 31 OO, while the bovine liver measured approximately 26 OO. Test results from this study for the softest material is roughly 76A, which would be approximately 100 on the OO scale. Therefore, the data gathered from this test indicates that the

TPU and TPE materials are too hard to achieve comparable surface hardness of those organs, although this does not imply that this cannot simulate the overall stiffness of the organ.

In addition to TPU and TPE materials, the selected resins were tested to determine their hardness with respect to the specified values for each material. The results presented in Table 4 summarize test results along with the percent difference between the measured and specified values.

**Table 4. Durometer test results for resin material.**

Material ID	Specified [SU]	Measured [SU] (SD)	Percent difference
Resin 80A	80	75.8 (3.3)	-5.2%
Resin 50A	50	57.3 (1.3)	14.6%
Resin 39A	39	80.1 (2.2)	105.4%

Notes: SU correspond to Shore units; SD: Standard Deviation

Test results summarized in Table 2 reveal that the Formlabs resins (Resin 80A and Resin 50A) are relatively close to their specified value, while Resin 39A (manufactured by Resione) shows a difference over 100%, indicating the true hardness is over double the specified value. These differences can be attributed to the following factors: printing settings, resin manufacturing methods, or the specific time in the manufacturing process at which the manufacturer measures hardness. The results obtained for the resin materials suggest that these factors will need to be taken into consideration in further tests when evaluating and comparing these materials.

#### 4.2.2 Cadaveric Organs

Five readings were collected and averaged at each location using a Shore O durometer, which falls between the OO and A scale, this recorded data is listed in Table 5.

**Table 5. O scale durometer test results for cadaveric specimens.**

Testing Site	Fixed hardness [SU] (SD)	Unfixed hardness [SU] (SD)	Percent difference
Forehead	46 (5.5)	36 (5.2)	27%
Temple	36 (6.0)	28 (12.3)	26%
Chin	42 (9.0)	33 (7.3)	28%
Heart	15 (5.1)	-----	-----
Lung	13 (5.7)	-----	-----
Liver	29 (10.1)	-----	-----

Notes: SU: Shore units; SD: Standard Deviation

This test showed that fixed organs are 26%-28% harder than unfixed organs, thus showing the variation between the hardness of fixed and unfixed cadaveric tissues. The hardest fixed tissue (46O or 33A) is approximately 57% softer than the softest candidate TPU and TPE material (76A).

### 4.3 Raw Filament Tensile Testing

Force-displacement and stress-strain curves obtained from tensile testing of raw filaments are compiled in Figure 17(a) and (b). These plots show a small elastic portion, in the range 0 to ~25 mm, followed by a long hyperelastic curve for the rest of the test. Hyperelastic materials do not exhibit a yield point like brittle materials such as alloys and hard plastics. Hyperelastic materials will continue to deform elastically until breaking. The strain values were calculated based on a gauge length of 100 mm. While the filament diameter may have decreased as testing occurred, the initial cross-sectional area is used in the calculation for engineering stress. To calculate this

value of stress, the force (N) was divided by the nominal cross-sectional area (diameter of 1.75 mm) of the specimen to determine the nominal tensile stress (MPa). This calculation can be seen in Eq. 2. Each maximum stress value and corresponding percent elongation for each material are shown in Table 6 where they are compared to the manufacturer’s technical data.

$$\frac{F}{A} = \sigma \quad \text{Eq. 2}$$

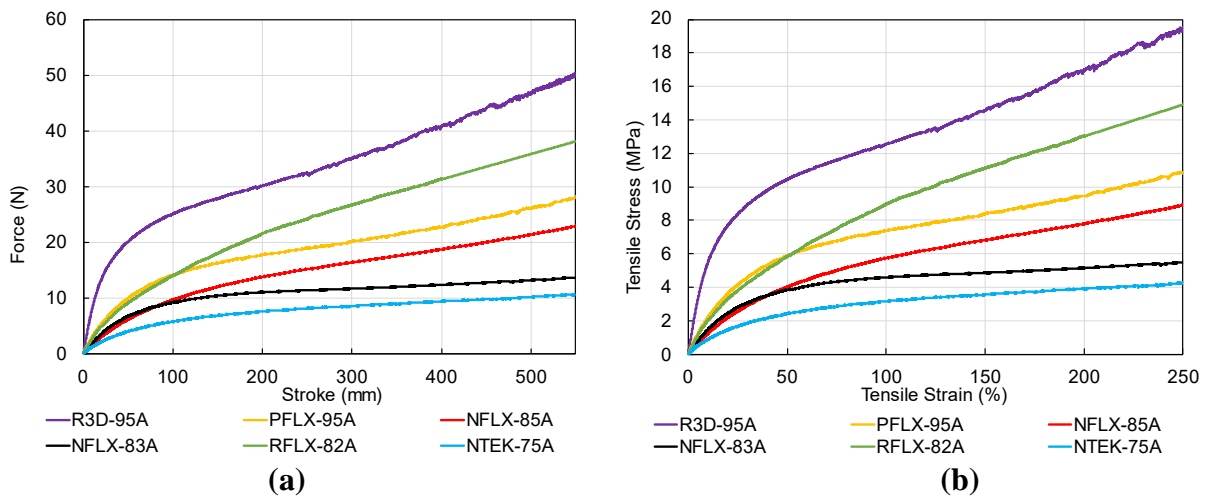


**Figure 17. Uniaxial raw filament testing results in terms of: (a) Force versus stroke plot (b) Engineering stress versus strain plot.**

**Table 6. Maximum stress values at respective elongation percentage.**

Material ID	Collected Data		Manufacturer Data	
	Elongation (%)	Max Stress [MPa] (SD)	Elongation at Break (%)	Tensile Strength (MPa)
R3D-95A	250	21.6 (0.3)	330	29.0
PFLX-95A	250	12.1 (0.2)	330	29.0
NFLX-85A	250	9.9 (0.1)	660	26
NFLX-83A	250	5.8 (0.1)	900	25
RFLX-82A	250	16.3 (NA)*	650	45
NTEK-75A	250	4.5 (0.1)	600	22

Notes: \*Only one specimen was tested; SD Standard Deviation.

When each filament was placed into the test fixture, the ends were tightened as much as possible to avoid slippage during the test. Although this was not always achievable, as the harder materials slipped out of the test fixture shortly after 250% elongation, whereas the softer materials slipped before breaking as well, typically after increased elongation. None of the materials tested in this experiment reached breaking points. However, for the purposes of this application, testing the material at its maximum elongation is not crucial.

#### **4.4 ‘Dog bone’ Tensile Testing**

Dog bone testing was conducted as described in section 3.5.3 with Figure 18 illustrating the results of the three print layer orientations of the tensile specimens for each material. A marked increase in the required force occurred as the material began to pull apart. After approximately 5 mm of elongation a slight decrease in required force was observed, followed by a steady increase. Across all orientations the required force was highest at 0° orientation, followed by 45° orientation, and then 90° orientation. This is due to the bonds between print layers being the weakest point of the specimen, and the layers being easier to separate at 90° orientation than at 0° orientation. The harder materials tested in this experiment were more prone to slippage from the test fixture before breaking. This is likely due to the harder materials compressing less in the clamp than the softer materials. The results compare the maximum stress and strain measurements for each print orientation.



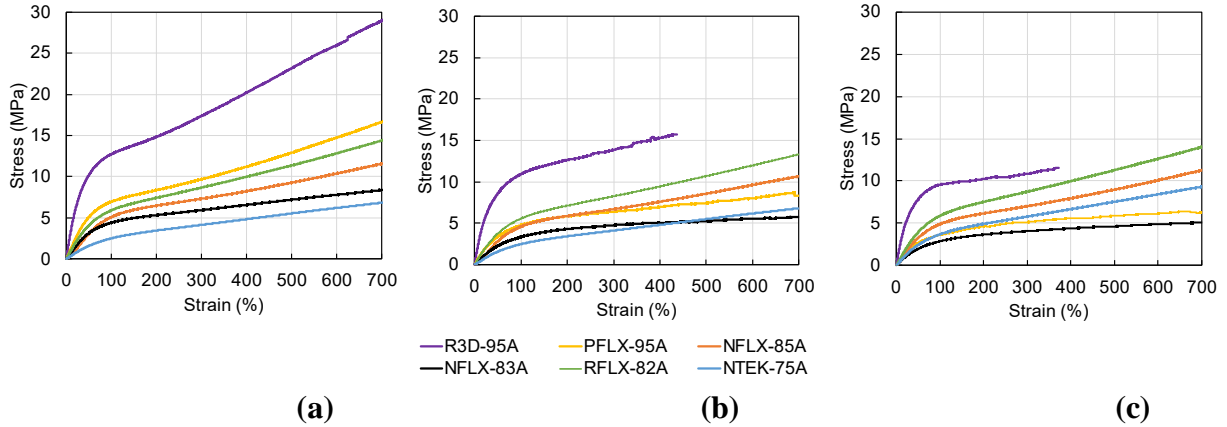


**Figure 18. Dog-bone tensile test results as function of specimen printing orientation: (a) 0°; (b) 45°; (c) 90°.**

Figure 19 shows the specimens after testing. The 45° and 90° print orientations experienced delamination between layers causing the specimen to break. Therefore, the figure shows the specimens breaking at 45° and 90° from the pulling direction. The strength of the bonds between print layers were tested on these specimens instead of testing the strength of the material. The 0° orientation truly tested the strength of the material, delamination between layers also occurred in these specimens, although it did not cause the ultimate failure. The 45° and 90° print orientations also failed at the base of the exposed specimen, where the clamp contacted the specimen.

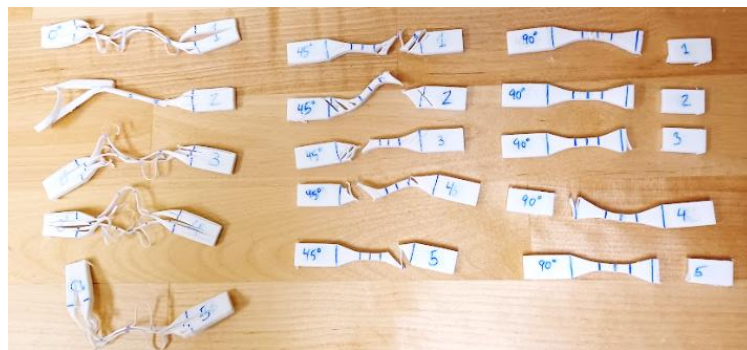


**Figure 19. (From left to right) 0°, 45°, 90° print orientation specimens after testing.**

Table 7 presents the maximum engineering stresses calculated at the maximum elongation achieved for each material. To obtain the value of stress, the force (N) was divided by the cross-sectional area (mm<sup>2</sup>) of the smallest portion of specimen (based on the original specimen dimensions) to determine the tensile engineering stress (MPa). All dimensions and geometries of the specimen are listed in section 3.5.3. The surface area of the square cross section was 10.24 mm<sup>2</sup>. This calculation can be seen in Eq. 2. As a comparison, Table 8 summarizes the ultimate stress and strain values for certain organs ranging from porcine, bovine, and human obtained from literature.

All print orientations of NTEK-75A, ranging from 7 MPa to 14 MPa, compare best with the pig kidney with maximum stresses of 6 MPa to 14 MPa (Farshad et al. 1999). Most values from this literature are less than the measurements taken from this testing. The lowest maximum stress value recorded in testing was the NFLX-83A 90° orientation with a value of 5 MPa. Although the 3D printing materials tested reached higher strain values than the organ specimens, the stress values are on the same order of magnitude.

**Table 7. Maximum stress values at percentage elongation at break.**

Material ID	Elongation At Break (%)	Max Stress 0° (MPa) (SD)	Elongation At Break (%)	Max Stress 45° (MPa) (SD)	Elongation At Break (%)	Max Stress 90° (MPa) (SD)
R3D-95A	723%	29 (0.5)	445%	16 (0.6)	369%	12 (0.6)
PFLX-95A	2341%	38 (0.9)	812%	9 (0.8)	1320%	9 (0.4)
NFLX-85A	2417%	25 (0.7)	2314%	23 (0.3)	1917%	20 (0.2)
NFLX-83A	1737%	13 (0.1)	1134%	7 (0.4)	738%	5 (0.1)
RFLX-82A	1969%	25 (0.4)	1969%	22 (0.4)	1969%	26 (0.6)
NTEK-75A	737%	7 (0.3)	947%	9 (0.1)	1227%	14 (0.1)

Notes: SD Standard Deviation.

**Table 8. Maximum stress values at respective elongation percentage for unfixed organs. (Snedeker et al. 2005)**

Reference	Biological Origin	Organ	Ultimate Stress (MPa)	Ultimate Strain (%)
Farshad et al. 1999	Pig	Kidney	6 - 14	18 - 45
Hollenstein et al. 2006	Cow	Liver	9.2	35
Snedeker et al. 2005	Pig	Kidney	10.9	41
	Human	Kidney	9.0	33.4
Stingl et al. 2002	Human	Liver	0.203	
Brunon et al. 2010	Human	Liver	1.85	32.6
	Pig	Liver	2.03	43.3

#### 4.5 Unconfined Compression

The plots in Figure 20 show a nonlinear steady increase in force across all infills due to the compression of the outer cylinder and the infill structure, followed by a small decrease in load caused by buckling of the specimen's outer walls. The cylindrical specimens under compression comprise a relatively thin external wall (1 mm thick) and infill with varying densities partially connected to the cylindrical wall and the top and bottom surfaces of the cylinder. In the classic linear buckling theory for cylinders under compression, the critical buckling load is controlled by the slenderness ratio, which is defined as the shell dimensionless thickness  $h = t/R$ , where  $t$  is the wall thickness and  $R$  is the cylinder radius, the modulus of elasticity  $E$  and the Poisson ratio of the material according to the following equation:  $\lambda = Eh / \sqrt{3(1 - \nu^2)}$ . (Timoshenko, 1914, Koiter 1945). When the compression load reaches a critical value, the shell buckles in the form of several dimples or periodic-like “wrinkles” along the cylinder's longitudinal axis. Buckling of the outer cylindrical portion of the specimens was more prevalent when the infill density was at 10%, which translated into relatively small peak loads, as shown in Figure 20(a). Higher infill

percentages followed a similar trend, but the higher infill percentages provided more internal support to the outer cylinder, which reduced the occurrence of buckling as the specimen behaved more like a solid cylinder.

Values listed in Table 9 are obtained through calculating stress and strain experienced by the specimen at the maximum load. To obtain the value of stress, the force (N) was divided by the cross-sectional area of the specimen (based on the original specimen dimensions) to determine the nominal compression stress. The cross-sectional diameter of the cylindrical specimen was 20 mm, which yields a surface area of 314.1 mm<sup>2</sup>. This calculation is given by Eq. 2. Strain was calculated as the cylinder height changed with respect to its original height (10 mm) as the cylinder compressed. The results compare the force required to compress each material for different infills. These calculations are also compared to human poroelastic articular cartilage, under similar testing conditions.

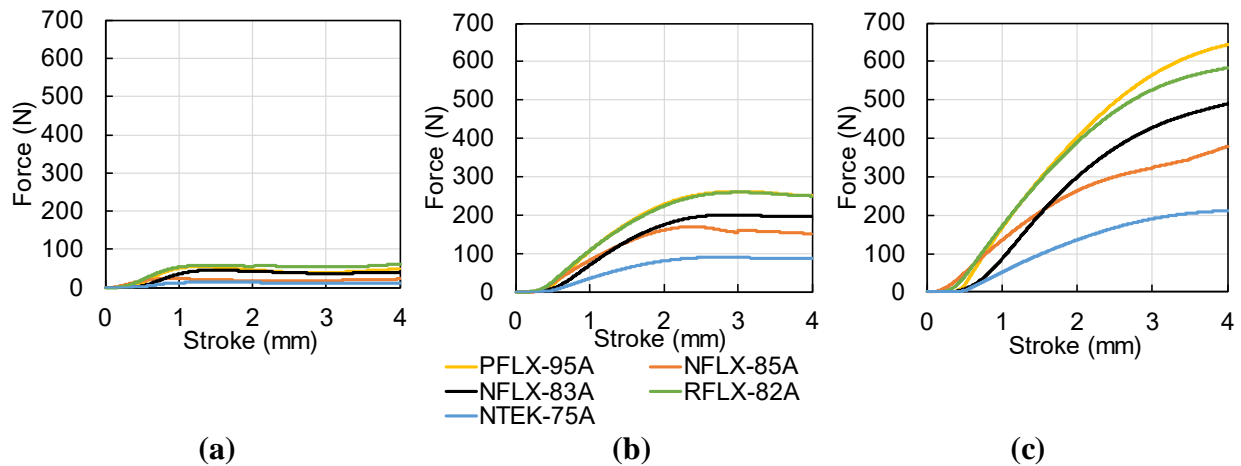


**Figure 20. Unconfined compression test results as function of infill percentage: (a) 10%; (b) 30%; (c) 50%.**

**Table 9. Stress and strain values for unconfined compression testing.**

Material ID	10% Infill		30% Infill		50% Infill	
	Max stress (MPa) (SD)	Strain	Max stress (MPa) (SD)	Strain	Max stress (MPa) (SD)	Strain
PFLX-95A	0.9*	0.4	0.9*	0.3	2.4*	0.5
NFLX-85A	0.1 (0.02)	0.1	0.6 (0.17)	0.2	1.3 (0.21)	0.4
NFLX-83A	0.2 (0.05)	0.1	0.7 (0.01)	0.3	2.0 (0.02)	0.5
RFLX-82A	0.2 (0.06)	0.2	0.9 (0.01)	0.3	2.2 (0.01)	0.5
NTEK-75A	0.1 (0.002)	0.2	0.3 (0.01)	0.5	0.8 (0.01)	0.5

Notes: \*Only one specimen was tested; SD Standard Deviation

Poroelastic articular cartilage is commonly used in biological research for its equilibrium response under compressive loading conditions. Boschetti (Boschetti et al. 2004) found compression stress values between 0.26 MPa to 0.50 MPa. Of the material tested and summarized in Table 9, NTEK-75A with 30% infill most closely agrees to Boschetti's data. This material and infill displayed the only compression stress values in range of the literature data. The higher percentage infill was measured to be too hard, and the lower percentage infill was too soft, with the exception of PFLX-95A with 10% infill being too high in the range. All other materials with the 30% infill were also too hard. Thus, meaning that the other materials, excluding the NTEK-75A, would benefit from an infill percentage ranging from 10% to 30%.

#### **4.6 Confined Compression**

The data collected from confined compression tests are compared to human tissue to assess the similarities of stiffness. The compression force-displacement curves shown in Figure 21 illustrate a small peak in force followed by an increase in force until the test is complete. This behavior occurs across the 10% and 30% infills, but not the 50% infill. This behavior is attributed to the compressibility of the specimen, which is controlled by the infill percentage,

similar to the unconfined compression test. The first force peak corresponds to buckling of the internal structure, followed by the compression of the material once the infill material has collapsed and bunched internally. The specimen is forced to buckle internally, because of the confined nature of the test. Compared to the unconfined compression testing, the buckling of the internal infill structure produced an inward buckle shape instead of an outward buckle in the perimetral cylinder. This buckling behavior is due to the lack of space to expand outwardly when the specimen is compressed under confined conditions. An example of this phenomenon can be seen in Figure 23. The higher percentage infill requires more force to compress due to the increased volume of material. The slenderness ratio is the same for these specimens as previously mentioned in section 4.5.

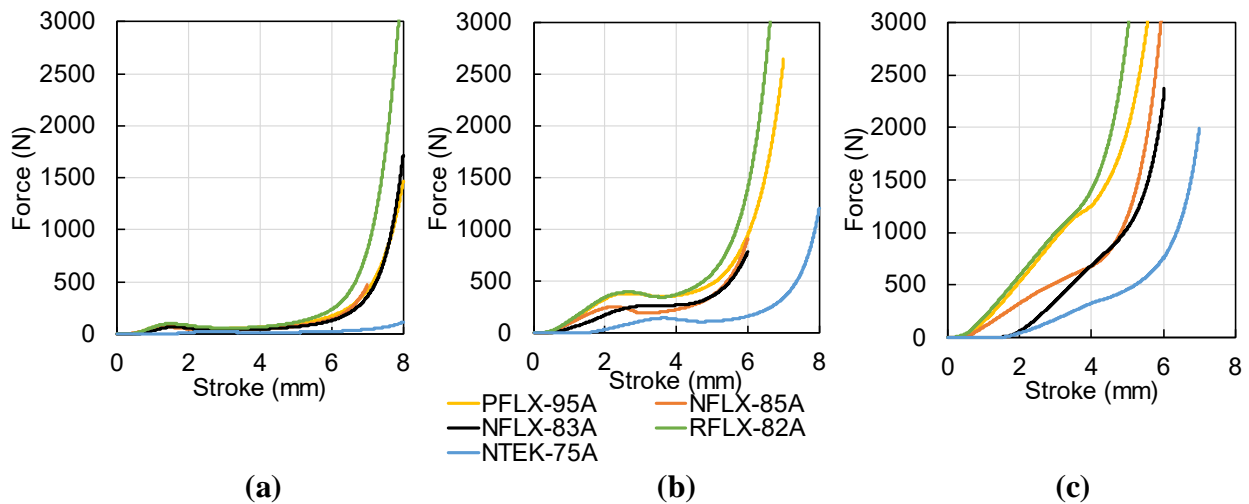


**Figure 21. Confined compression test results as function of infill percentage: (a) 10%; (b) 30%; (c) 50%.**



**Figure 22. Buckled specimen after confined compression testing.**

To determine the nominal or engineering compression stress in MPa, the force (N) was divided by the cross-sectional area of the specimen (based on the original specimen dimensions). This calculation is given by Eq. 2. The surface area of the circular cross section was 314.1 mm<sup>2</sup>.

**Table 10. Stress and strain values for confined compression testing.**

Material ID	10% Infill		30% Infill		50% Infill	
	Max stress [MPa] (SD)	Strain	Max stress [MPa] (SD)	Strain	Max stress [MPa] (SD)	Strain
PFLX-95A	0.3 (NA)*	0.2	1.3 (NA)*	0.3	6.8 (NA)*	0.5
NFLX-85A	0.3 (0.08)	0.1	0.9 (0.04)	0.2	4.0 (0.09)	0.5
NFLX-83A	0.3 (0.02)	0.2	0.9 (0.20)	0.3	3.6 (0.06)	0.5
RFLX-82A	0.3 (0.09)	0.2	1.4 (0.12)	0.3	10.0 (0.08)	0.5
NTEK-75A	0.1 (0.003)	0.3	0.5 (0.02)	0.4	1.6 (0.02)	0.5

Notes: \* Only one specimen was tested; SD Standard Deviation.

The study conducted by Boschetti, et al. (2004) recorded data for confined compression testing, with average stress ranging between 0.27 MPa and 0.51 MPa. The measurements collected in this research, listed in Table 10, confirms the results from the previous section that the closest value to Boschetti's data comes from the 10% infills of all materials except the NTEK-75A. NTEK-75A, whose 10% infill data was out of range from the literature, is in range at 30% infill. These results show that harder materials with low infills exhibit similar stiffness to softer materials with higher infills. The softer material with a higher infill would create a more uniform model as opposed to a model with a harder outer shell.

#### 4.7 Scalpel Puncture Test

The scalpel puncture test was designed specifically to reproduce a surgical puncture that precedes a surgical incision. Results for synthetic materials tested, compiled in Figure 23, show a relatively steady increase in force due to the bending of the top cylindrical surface under the

force of the scalpel before penetrating the surface. Subsequent peaks occur when the scalpel begins cutting each layer of infill. Results presented in Figure 23 also show that the force required to puncture the outer wall increases as infill percentage increases, due to increased volumetric density. This is shown by the stroke at which the puncture occurs, the higher the stroke, the more deformation has occurred before puncture. As expected, the harder materials, determined from the durometer test, required more force to penetrate the outer wall. Table 11 compiles the force at the first peak and the corresponding stroke at which it occurred for each material and infill density.

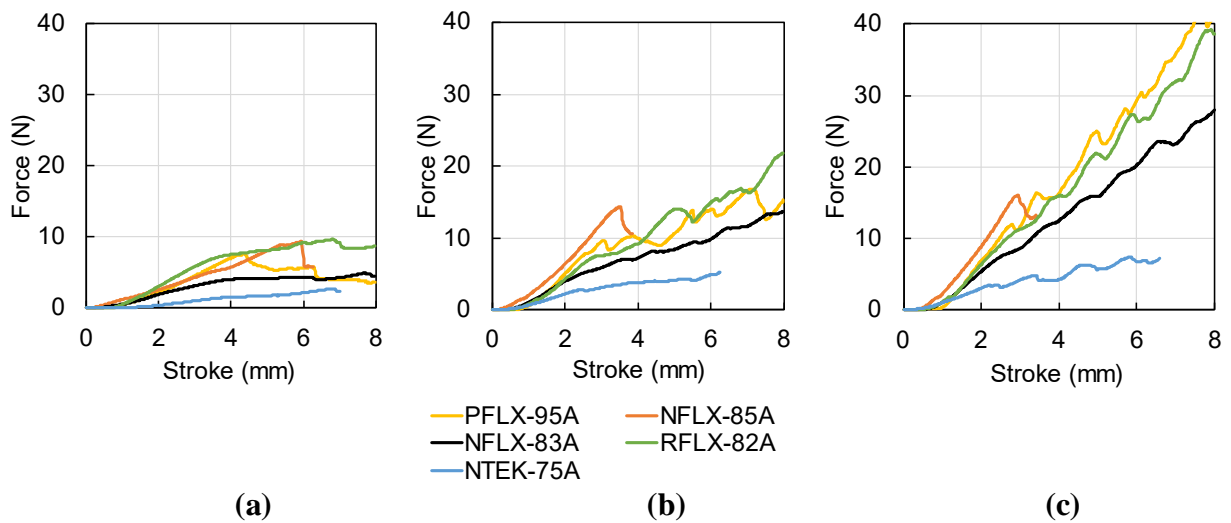


**Figure 23. Scalpel puncture test results as function of infill percentage: (a) 10%; (b) 30%; (c) 50%.**

**Table 11. Scalpel puncture test force required to puncture outer wall.**

Material ID	10% Infill		30% Infill		50% Infill	
	Force [N] (SD)	Stroke (mm)	Force [N] (SD)	Stroke (mm)	Force [N] (SD)	Stroke (mm)
PFLX-95A	7.6 (NA)*	4.4	9.2 (NA)*	3.1	11.9 (NA)*	2.8
NFLX-85A	9.3 (1.1)	6.0	14.2 (0.2)	3.5	15.9 (1.3)	3.0
NFLX-83A	4.3 (0.5)	6.1	5.8 (0.5)	2.4	7.9 (0.6)	2.7
RFLX-82A	9.7 (0.5)	6.8	7.5 (0.8)	3.0	11.4 (0.9)	3.1
NTEK-75A	2.7 (0.4)	6.9	2.6 (0.5)	2.5	3.5 (0.8)	2.4

Notes: \*Only one specimen was tested; SD Standard Deviation.



This test was also performed with the selected resin materials. The peak force occurred at the maximum stroke (8 mm) because of the solid infill (see Figure 24.) Since resin materials have no internal structure or ‘outer wall’, unlike the FDM materials, there is little compression before penetration. The maximum force, seen in Figure 24, for Resin 80A was 100.4 N, Resin 50A was 41.5 N, and Resin 39A was 173.1 N. This is consistent with the difference seen in the measured hardness values and the manufacturer’s specified hardness (Table 4). These results indicate that solid 50A is the most comparable resin to RFLX-82A or PFLX-95A at 50% infill. Both materials indicated that a ~40 N force would be required at 8 mm stroke. This result allows for a more direct comparison between TPU/TPE and resin-based materials in scalpel puncture testing.

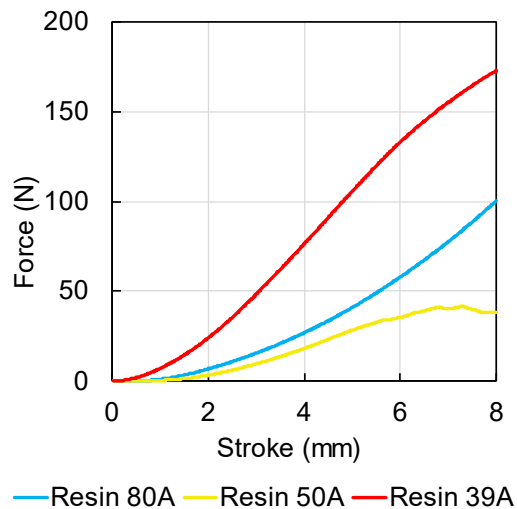


**Figure 24. Scalpel puncture test for all resin materials.**

Synthetic material test results were also compared to experimental results obtained from fresh porcine organs and tissues tested using the same testing method and conditions. Unlike the synthetic material, porcine organs and tissues tested do not have infills, but a non-negligible deformation to the tissue before puncture would still be expected. The force-displacement curves obtained from this test are shown in Figure 25. A subset of the data is shown in Figure 26 which

excludes skin data in order to expand the scale for clarity. Other than the skin tissues, all porcine organs tested behaved similarly.

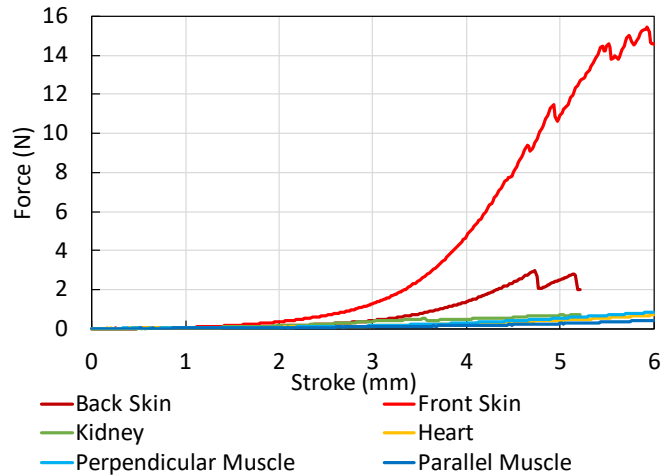


**Figure 25. Scalpel puncture test results for all porcine organs.**

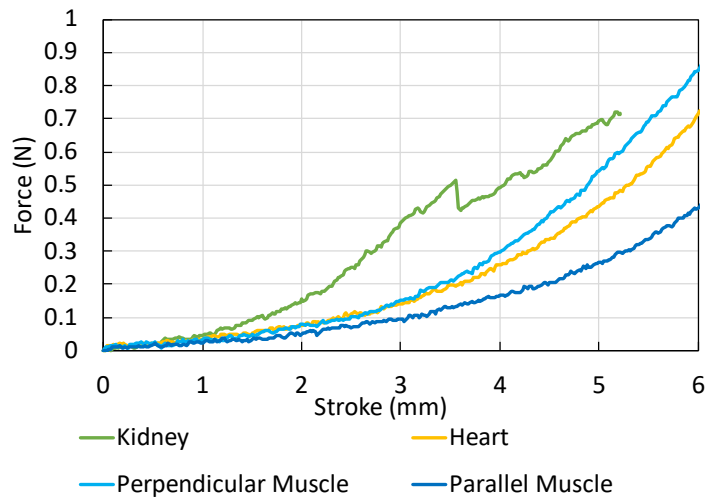


**Figure 26. Scalpel puncture test results for porcine kidney, heart, and muscle tissue.**

The outer (front) side of the skin was harder than the inside (back) skin and other organs. The comparative muscle tissues required different levels of cutting force with the fibers perpendicular to the scalpel blade requiring a higher force to penetrate. This was expected as this trend has been common with 3D print orientations where the scalpel cuts between layers, as opposed to

across layers. Heart tissue exhibited similar trends to the muscle tissues and the kidney. A small drop in required cutting force was observed for the kidney around the 3.5 mm stroke length, possibly due to the scalpel cutting softer tissue or a void within the kidney structure. The forces at mid-stroke (3 mm) and maximum stroke (6 mm) were compiled in Table 12. These maximum forces are taken from the same test at different stroke lengths. The data shows synthetic 10% infill material is stiffer than fresh porcine tissue requiring almost twice the puncture force, and a softer synthetic material would be required to obtain similar mechanical properties.

**Table 12. Scalpel puncture test results for porcine tissues and organs.**

Organ	Stroke 3 mm	Stroke 6 mm	Standard Deviation (N) (SD)
	Force (N)	Force (N)	
Back of Skin	0.4	2.7	0.4
Front of Skin	1.3	14.5	0.5
Kidney	0.4	0.7	0.2
Heart	0.1	0.7	0.1
Perpendicular Muscle	0.2	0.9	0.2
Parallel Muscle	0.1	0.4	0.1

Notes: SD Standard Deviation.

## 4.8 Needle Puncture Test

Needle puncture testing was performed as described in section 3.5.6. Data collected from this experiment is compared across infills and materials and compared to tests reported by Maurin et al. (2004) on various porcine organs. Figure 27 illustrates a steady increase in force across all infills which is due to the bending of the outer wall under the force of the needle before penetration.

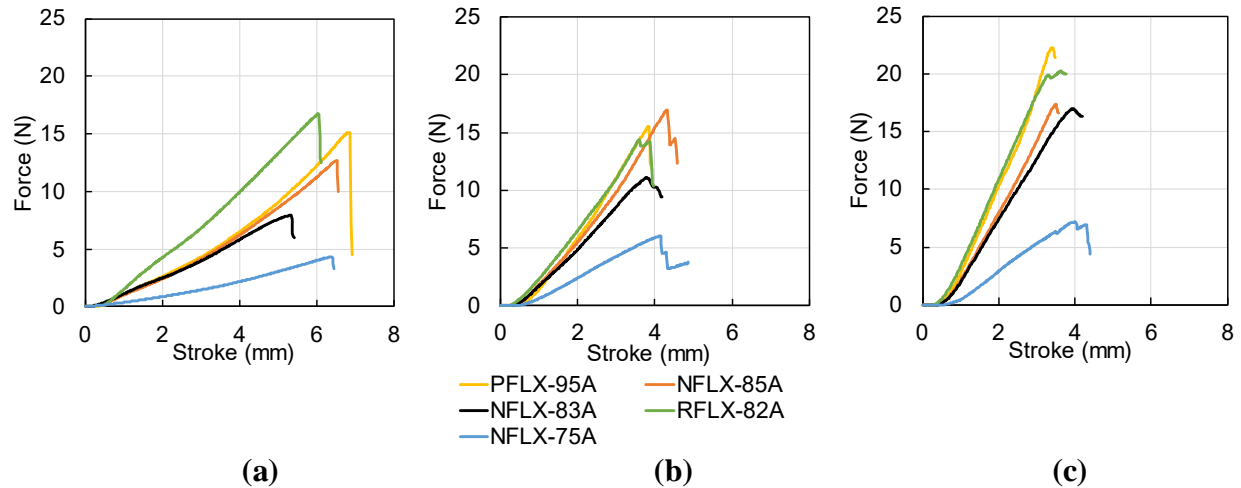


**Figure 27. Needle puncture test results as function of infill percentage: (a) 10%; (b) 30%; (c) 50%.**

Once the force exceeds the level required to puncture the surface, the needle penetrates the outer wall and enters the infill of the specimen, decreasing the force suddenly. Load-displacement curves show that the peak forces required to puncture the outer wall increase with increasing infill density and volume density which result in greater wall support. This behavior is also shown by the stroke at which the puncture occurs with higher stroke indicating greater deformation before puncture. As expected, harder materials require more force to penetrate the outer wall. Table 13 compiles the maximum forces and strokes at which they occurred for each infill and each material.

**Table 13. Needle puncture test force values for all infill percentages.**

Material ID	10% Infill		30% Infill		50% Infill	
	Force [N] (SD)	Stroke (mm)	Force [N] (SD)	Stroke (mm)	Force [N] (SD)	Stroke (mm)
PFLX-95A	15.1 (NA)*	6.8	15.6 (NA)*	3.8	22.3 (NA)*	3.4
NFLX-85A	12.7 (0.9)	6.5	16.9 (1.8)	4.3	17.4 (1.0)	3.5
NFLX-83A	7.9 (0.8)	5.4	11.1 (1.0)	3.8	17.0 (1.1)	3.9
RFLX-82A	16.7 (1.4)	6.0	14.4 (1.8)	3.6	20.3 (1.3)	3.6
NTEK-75A	4.3 (0.1)	6.4	6.0 (0.8)	4.1	7.2 (1.6)	4.0

Notes: \*Only one specimen was tested; SD Standard Deviation.

As a point of comparison, a needle puncture test conducted by Maurin et al. (2004) used an 18-gauge biopsy needle on various fresh organs in living, anesthetized pigs. This needle is slightly larger than the 20-gauge needle used in this study. Table 14 and Table 15 compile the tests results obtained from manual needle insertion performed by a radiologist and results obtained from a robotic insertion as reported by Maurin.

**Table 14. Manual Insertions, reformatted from Maurin et al. 2004.**

Organs and method (# trials)	Maximum force (N)	Std. deviation (N)
Liver, with skin (10)	3.73	0.59
Liver removal, with skin (10)	2.33	0.32
Liver, direct access (6)	0.7	0.29
Liver Capsule, direct access (6)	0.23	0.04
Liver removal, direct access (6)	0.3	0.28
Kidney, direct access (5)	0.74	0.54
Pancreas, direct access (5)	0.83	0.28

**Table 15. Robotic Insertions, reformatted from Maurin et al. 2004.**

Organs and method (# trials)	Maximum force (N)	Std. deviation (N)
Liver, with skin (6)	1.89	0.36
Liver removal, with skin (6)	0.69	0.28
Liver, direct access (6)	0.59	0.17
Liver Capsule, direct access (6)	0.35	0.12
Liver removal, direct access (6)	0.17	0.06
Kidney, direct access (4)	1.22	0.34

The material that exhibits the closest needle exertion force to the porcine liver with skin test from Maurin et al. 2004 is NTEK-75A with 10% infill with a 13.7% percent difference. These tests are likely most relevant in assessing material suitability in this application. Test results obtained with pig tissues, which are similar to human tissues, indicate that the materials and infills chosen in this research are too stiff for this specific soft tissue comparison.

## 4.9 Scalpel Cutting Test

Scalpel cutting testing is described in section 3.5.7. The first set of scalpel cutting tests utilizes two cutting configurations: a superficial cut (1 mm depth) and a deep cut (6 mm depth) as shown in Figure 28. These set of tests were conducted with a #22 surgical blade. Graphs presented in Figure 29 and Figure 30 compile the averaged curves corresponding to the 1 mm-depth cut and the 6 mm-depth cut for each material and infill percentage selected for this research.

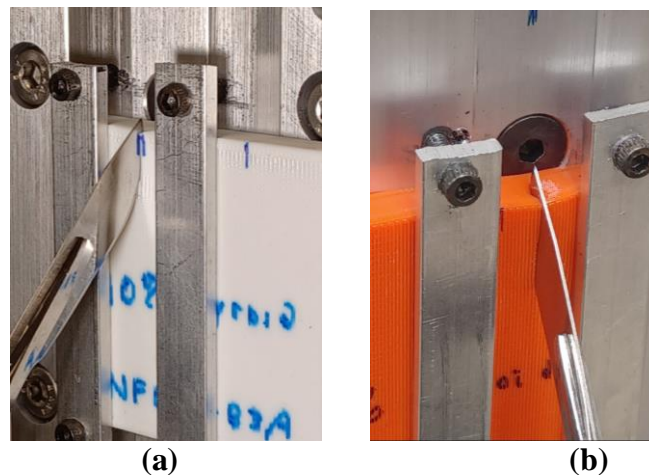


**Figure 28. Scalpel cutting tests (a) Superficial (1 mm) cut. (b) Deep (6 mm) deep cut.**

Results compiled in Figure 29 and Figure 30 show the cutting force increasing nearly linearly to an initial peak which corresponds to the force necessary to cut through/into the outer wall of the specimen. This outer wall is partially pushed and deformed by the blade before initial cutting, creating a small increase in force recorded. Once the outer wall cut has been initiated, the force plateaus corresponding to the cutting of the midsection of the specimen. The length of the plateau corresponds to the specimen length (50 mm) with small peaks in the plateau region likely caused

by cutting internal structures associated with the infill support. The final peaks correspond to the blade pushing the outer wall as it exits the specimen.

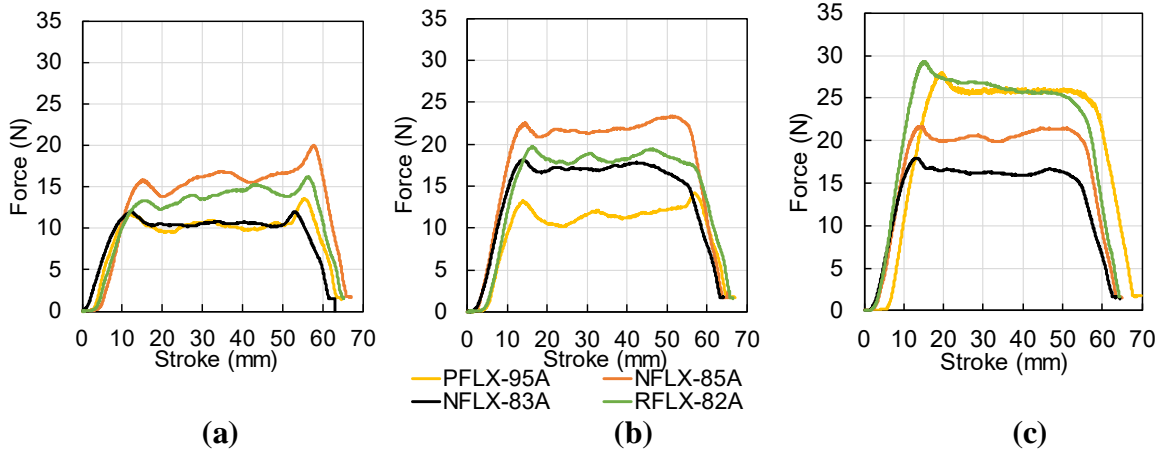


**Figure 29. Scalpel cutting test at 1 mm depth of cut results as function of infill percentage: (a) 10%; (b) 30%; (c) 50%.**

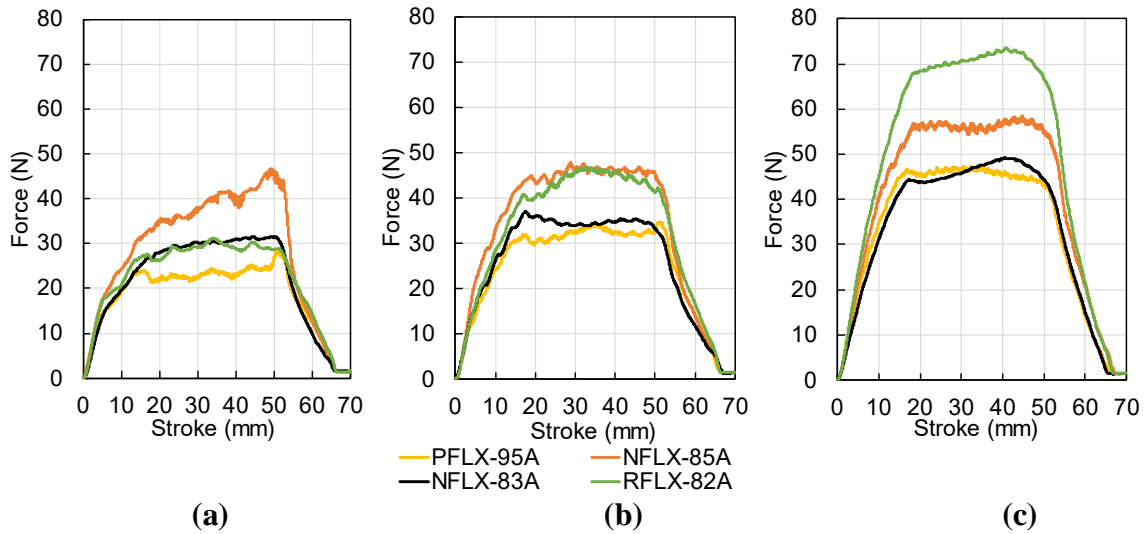


**Figure 30. Scalpel cutting test at 6 mm depth of cut results as function of infill percentage: (a) 10%; (b) 30%; (c) 50%.**

As expected, results in Figure 30 show that as depth of cut increases (from 1 to 6 mm), so does the required force to cut the material as the blade is in contact with more material in the deeper cut. This is reflected in the average plateau values. Additionally the 6 mm depth cut data

exhibits increased amplitude variation in the plateau region than the 1 mm cut, due to the scalpel cutting through multiple inconsistent layers of the infill, as opposed to the 1 mm depth that is only deep enough to cut through the outer wall. Table 16 summarizes the average cutting forces for each material and percentage of infill.

**Table 16. Superficial and deep scalpel cutting depths with average forces by infill percentages and material types.**

Material ID	1 mm cutting depth			6 mm cutting depth		
	Average Force 10% Infill [N] (SD)	Average Force 30% Infill [N] (SD)	Average Force 50% Infill [N] (SD)	Average Force 10% Infill [N] (SD)	Average Force 30% Infill [N] (SD)	Average Force 50% Infill [N] (SD)
PFLX-95A	10.4 (0.4)	11.5 (0.5)	25.9 (0.4)	23.5 (1.6)	31.8 (1.6)	44.7 (2.0)
NFLX-85A	15.9 (0.3)	22.0 (0.5)	20.6 (0.5)	38.7 (2.4)	44.6 (1.6)	55.2 (2.2)
NFLX-83A	10.6 (0.4)	17.0 (0.5)	16.2 (0.8)	29.5 (0.7)	33.9 (1.3)	45.2 (1.6)
RFLX-82A	14.0 (0.7)	18.4 (0.6)	26.3 (0.9)	28.6 (1.4)	42.8 (1.6)	68.7 (3.6)

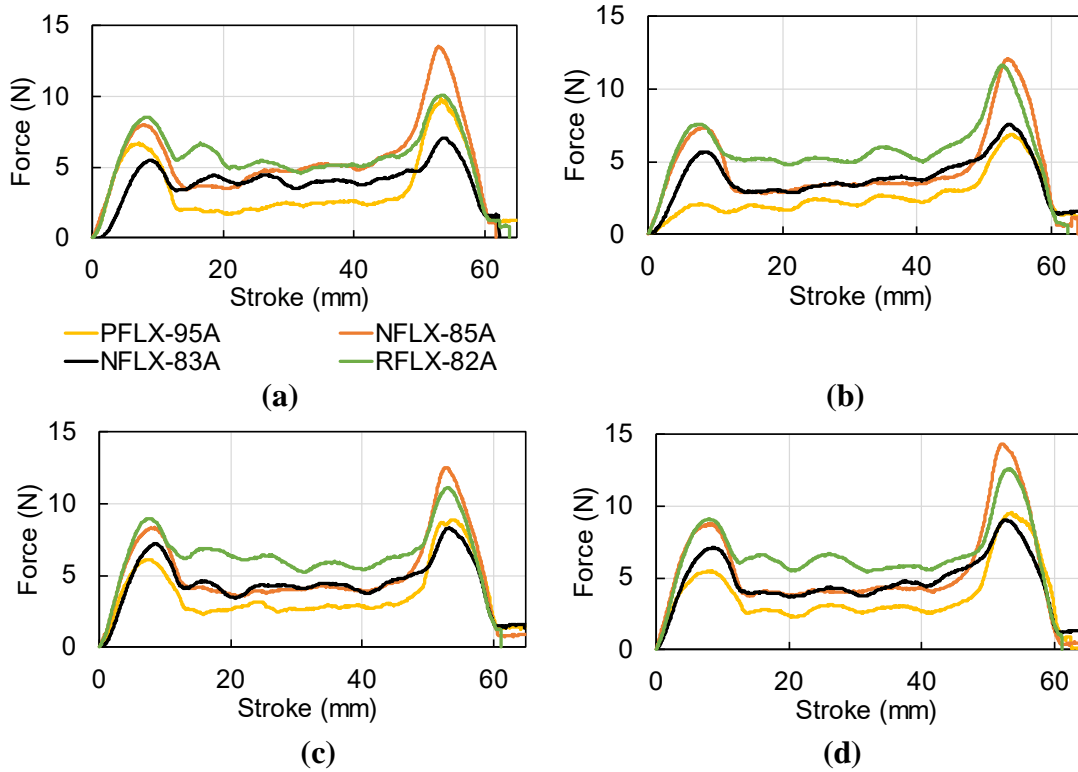
Notes: SD Standard Deviation.

A second set of specimens were tested to evaluate the cutting force as a function of external layer direction using a 4% square infill, previously explained in section 3.5.7. Four positions were tested: (a) 0° linear orientation (0° L) (b) 90° linear orientation (90° L) (c) 90° X-hatch orientation (90° X) (d) 45° X-hatch orientation (45° X). Measurements were taken during superficial and deep cuts and results are compiled in Figure 31 and Figure 32, respectively. The peaks seen in these figures are likely caused by the lack of support of the outer wall from the internal structure. Although infill effects are reduced, the supports on the attached areas under the outer wall still result in small variations and inconsistencies throughout the test. As the blade cuts 6 mm deep, the material still experiences deformation, although the blade is forced through the material. The cutting force required increases due to both the increased cut depth and the material deformation as the blade slices entirely through the specimen. Table 17 and Table 18

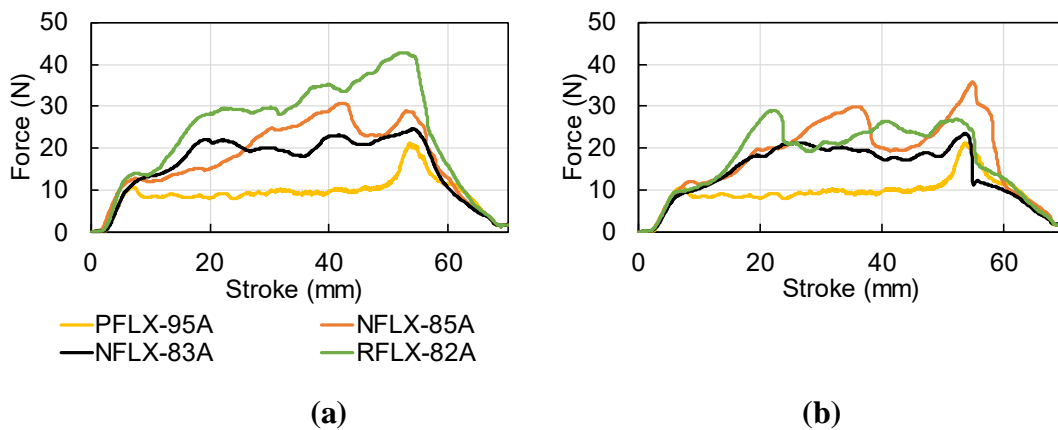


contain average cutting forces from the superficial and deep scalpel cutting tests, respectively.

Both tables compare the four print layer directions.



**Figure 31. Scalpel cutting test results for specimens with 4% infill and 1 mm depth of cut as a function of print layer direction: (a) 0° linear orientation (b) 90° linear orientation (c) 90° X-hatch orientation (d) 45° X-hatch orientation.**



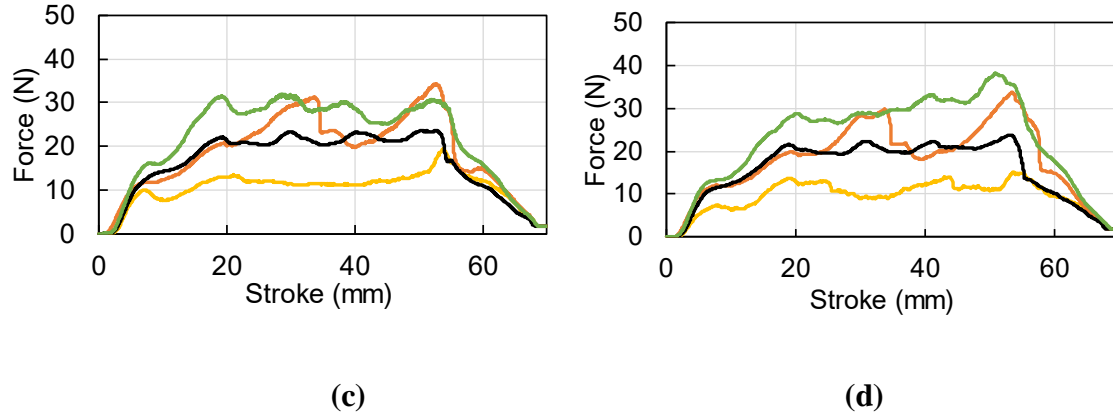


**Figure 32. Scalpel cutting test results for specimens with 4% infill and 6 mm depth of cut as a function of print layer direction: (a) 0° linear orientation (b) 90° linear orientation (c) 90° X-hatch orientation (d) 45° X-hatch orientation.**

**Table 17. Scalpel cutting depth (1mm) with average forces with 4% infill as a function of print layer directions.**

Material ID	Average Force 0° L [N] (SD)	Average Force 90° L [N] (SD)	Average Force 90° X [N] (SD)	Average Force 45° X [N] (SD)
PFLX-95A	3.6 (0.5)	2.8 (1.5)	3.9 (1.0)	4.0 (0.8)
NFLX-85A	6.0 (1.4)	4.8 (1.5)	5.5 (0.2)	5.9 (0.4)
NFLX-83A	4.4 (0.5)	4.2 (0.3)	5.0 (0.4)	5.2 (0.4)
RFLX-82A	6.2 (3.1)	6.3 (1.0)	6.8 (2.0)	7.0 (1.1)

Note: SD Standard Deviation

**Table 18. Scalpel cutting depth (6mm) with average forces with 4% infill as a function of print layer directions.**

Material ID	Average Force 0° L [N] (SD)	Average Force 90° L [N] (SD)	Average Force 90° X [N] (SD)	Average Force 45° X [N] (SD)
PFLX-95A	13.8 (2.2)	10.5 (0.8)	12.5 (1.1)	11.6 (1.6)
NFLX-85A	22.8 (4.4)	23.3 (3.9)	24.3 (3.1)	23.1 (3.5)
NFLX-83A	20.9 (1.0)	18.6 (2.1)	21.1 (1.6)	20.4 (1.4)
RFLX-82A	32.3 (1.5)	23.0 (2.0)	28.3 (2.0)	29.8 (2.2)

Note: SD Standard Deviation

The orientation requiring the lowest cutting force amongst materials tested was the 90°-linear orientation. The material that required the lowest cutting force was PFLX-95A for all print layer orientations, averaging 3.6 N and 9.6 N for the superficial and deep cuts, respectively. The second material was the NFLX-83A for all print layer orientations averaging 4.7 N and 20.3 N for the superficial and deep cuts, respectively.

A third set of specimens were tested to analyze the effect of the surface finish and external layer orientation. Specimens for this set were printed with a 10% infill density and cut with a 1 mm depth. Data shown in Figure 34 was acquired with the orientation of the scalpel blade either parallel or perpendicular to the deposited 3D print layer.

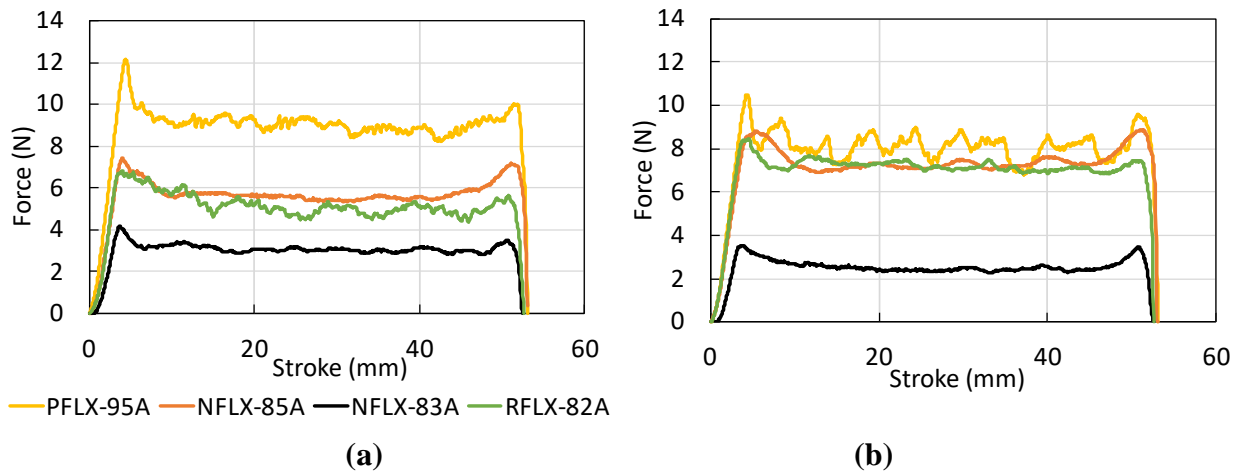


**Figure 33. Scalpel cutting test with (a) perpendicular lines to the direction of the cut. (b) parallel lines to the direction of the cut.**

The average force required by all materials in both external layer orientations can be seen in Table 19. The results from this test show a significant difference between cutting directions, with a maximum difference of approximately 2 N for specimens printed with RFLX-82A. Some materials, PFLX-95A and NFLX-83A, exhibited a lower required cutting force in the parallel

orientation while others experienced a lower cutting force, NFLX-85A and RFLX-82A, in the parallel direction. During these tests it was observed that the blade began to deflect resulting in cross cutting of print layers and altering the required cutting force. An example of this can be seen in Figure 34.

**Table 19. Perpendicular and parallel cut direction average force values.**

Material ID	Perpendicular Average Force [N] (SD)	Parallel Average Force [N] (SD)	Percent Difference
PFLX-95A	9.1 (1.0)	8.1 (0.9)	12.4%
NFLX-85A	5.8 (0.2)	7.4 (0.3)	-21.6%
NFLX-83A	3.1 (0.2)	2.5 (0.1)	24.0%
RFLX-82A	5.2 (0.3)	7.2 (0.2)	-27.8%

Notes: SD Standard Deviation.



**Figure 34. Scalpel cross cutting parallel print layers of the specimen.**

Additionally, all resins presented in Chapter 3 were tested using superficial cuts in solid infills. As previously mentioned in Table 4, the Resin-39A does not agree with the manufacturer’s specified hardness, with over a 100% difference. Therefore, the force data measured from this material may not be accurate. Figure 35(a) illustrates data collected from cutting resin material with a #22 surgical blade while (b) compares data collected from resins along with FDM materials cut with #11 surgical blade.

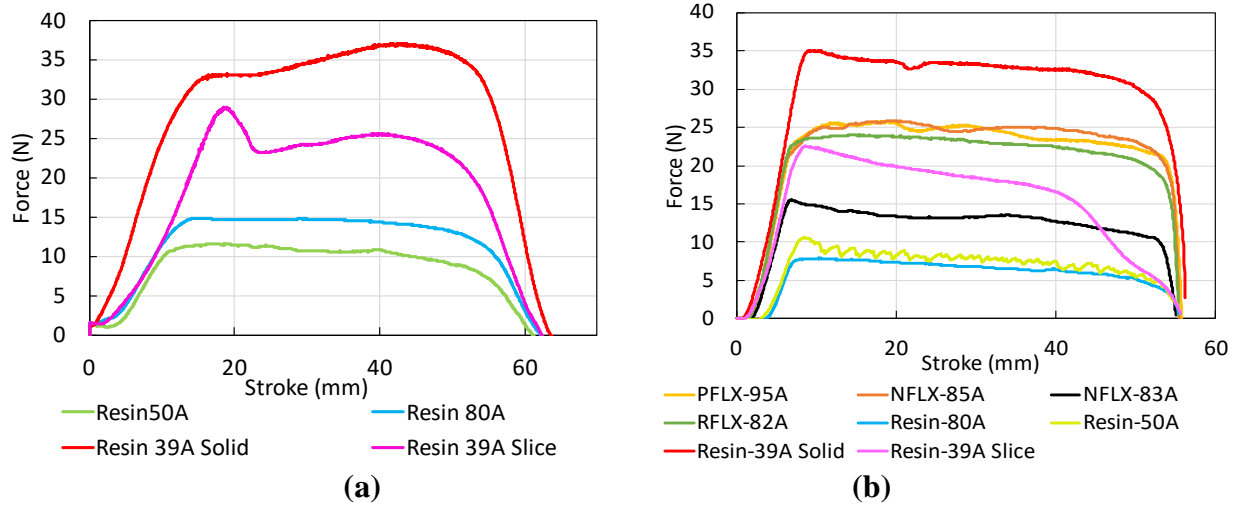


**Figure 35. (a) Scalpel cutting test at 1 mm deep for resins with #22 blade; (b) Scalpel cutting test at 1 mm deep for all synthetic materials including TPUs, TPEs, and resins with #11 blade.**

Resin-80A and Resin-50A were softer than the FDM materials. The scalpel cutting test results suggest that the Formlabs SLA printing is capable of printing softer materials than the Raise3D FDM printer. Table 20 compares the average cutting forces obtained with #22 and #11 blades. Both blades are commonly used in medical practices. The #22 surgical blade is typically used for rapid movements and dissection of larger structures, while the #11 blade is optimal for precise incisions and dissection of fine detailed structures. The ability to use different types of surgical blades on these synthetic organs increases their usefulness in medical training.

**Table 20. Average cutting forces for resin materials using #22 and #11 blades.**

Material ID	#22 Blade [N] (SD)	#11 Blade [N] (SD)
Resin 80A	14.1 (1.3)	6.4 (0.2)
Resin 50A	10.5 (2.5)	7.4 (0.4)
Resin 39A Slice	32.5 (5.2)	16.1 (0.6)
Resin 39A Solid	34.2 (3.9)	32.3 (0.7)

Notes: SD Standard Deviation.

The synthetic material cutting data was compared with results obtained from fresh porcine organs and tissues using the same testing method and conditions. Specimens of each organ were cut into slices of approximately 6 mm thickness, similar to synthetic materials. The same porcine organs were used as the comparative scalpel puncture test described in section 3.5.5. This test was conducted with a #22 surgical blade and the data collected from this test is shown in Figure 36. The porcine tissues are considerably softer compared to all synthetic materials tested in this study. Results shown in Figure 35(b) indicate that Resin 50A and Resin 80A both averaged roughly 7 N. Fresh organs average between 1 to 2 N, excluding the “Front Skin” which averaged roughly 4 N, as shown in Figure 36. The most comparable FDM synthetic material was NFLX-83A with 10% infill seen in Figure 35(b). This material displayed the closest results to fresh organs for the same cutting depth exhibiting an average cutting force of roughly 13 N shown in Figure 35(b).

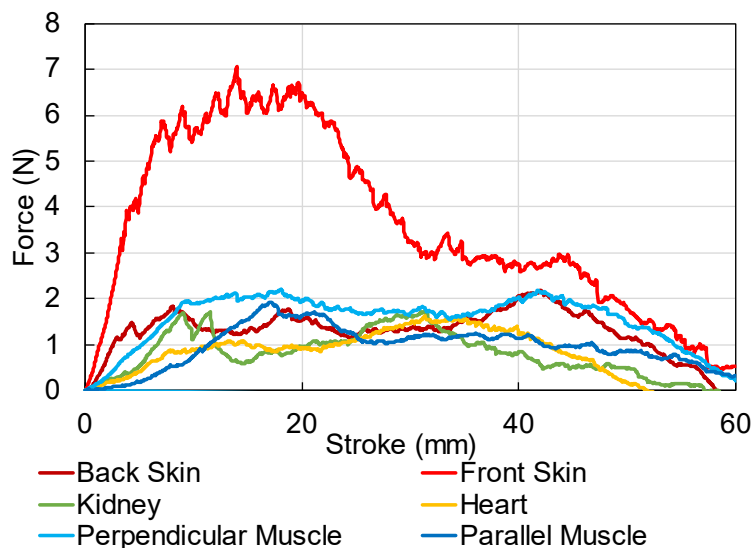


**Figure 36. Scalpel cutting test at approximately 4 mm deep for porcine organs and tissues.**

## 4.10 Friction Test

Friction tests were conducted on specimens of TPU/TPE materials as described in Section 3.5.8. The plots in Figure 37 shows two external print layer orientations, each with a linear increase of force until reaching an initial peak, which corresponds to the static friction force. Once this force was overcome, the specimen began sliding across the plate. This is followed by a small force decrease, becoming nearly constant, indicating the kinetic frictional force. Finally, the plot returns to equilibrium once the sliding stops. The ratio between the horizontal peak force and the normal force  $N$  (produced by a 1 kg mass and multiplied by gravity  $9.81 \text{ m/s}^2 = 9.81 \text{ N}$ ) applied to the specimen is the static friction coefficient of the material against the glove. This calculation can be seen in Eq. 3.

$$\frac{F_s}{N} = \mu \quad \text{Eq. 3}$$

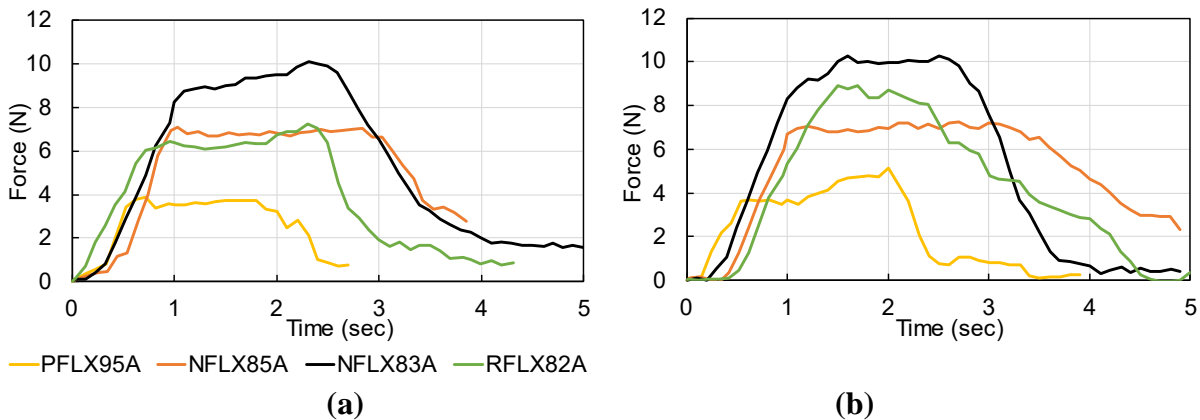


**Figure 37. (a) Parallel 3D print orientation relative to pulling direction. (b) Perpendicular 3D print orientation relative to pulling direction.**

**Table 21. Parallel 3D print orientation data table for friction testing.**

Material ID	Peak Sliding Tangential Force [N] (SD)	Normal Force [N]	Friction ( $\mu$ )
PFLX-95A	3.9 (1.4)	10	0.39
NFLX-85A	7.1 (0.8)	10	0.71
NFLX-83A	8.9 (1.2)	10	0.89
RFLX-82A	6.4 (1.7)	10	0.64

Notes: SD Standard Deviation.

**Table 22. Perpendicular 3D print orientation data table for friction testing.**

Material ID	Peak Sliding Tangential Force [N] (SD)	Normal Force [N]	Friction ( $\mu$ )
PFLX-95A	3.7 (1.6)	10	0.37
NFLX-85A	7.0 (0.9)	10	0.70
NFLX-83A	9.2 (3.5)	10	0.92
RFLX-82A	8.9 (2.4)	10	0.89

Notes: SD Standard Deviation.

According to The Engineering ToolBox, the range of static coefficients of friction for plastics are between 0.3 and 0.4 (The Engineering ToolBox). A low coefficient of friction value indicated that there is a small amount of force required to slide the material across a surface. Thus, the most frictional material is the NFLX-83A where the least frictional is PFLX-95A. PFLX-95A experienced a 5.4% difference between the print layer directions followed by NFLX-85A with a 1.4% difference, NFLX-83A with a -3.3% difference, and finally RFLX-82A with the largest difference of -28.1%.

Commonly when handling organs, they are wet and slippery due to natural lubricants and water content (University of Illinois, 1945). This data was collected in dry conditions because artificial training materials do not need preservatives or lubricants to maintain the health of the surrogate organ. Although this opens opportunities for future work in testing friction of synthetic materials in wet conditions.



## Chapter 5. Surrogate Organ 3D-Printing and Cutting Testing

### 5.1 Introduction

This chapter presents the test setup and results of the surrogate organ cutting pilot test and the participant survey that followed.

### 5.2 Surrogate Organ Prototype and Survey Design

After thorough analysis of all material characterization test data presented in the previous chapters, and comparison to literature, NFLX-83A was selected as a suitable candidate material for the surrogate organ prototypes. The organ selected for prototyping was the human tonsil due to its geometric simplicity, size, and internal structure. A pre-existing digital model (from JoePKrcma on Thingiverse.com) was adopted for 3D printing the prototypes for testing. The prototypes included a small tumor-like insert which was made of NFLX-85A to provide visual contrast to the NFLX-83A. This model is shown in Figure 38 and is roughly 5 cm long.

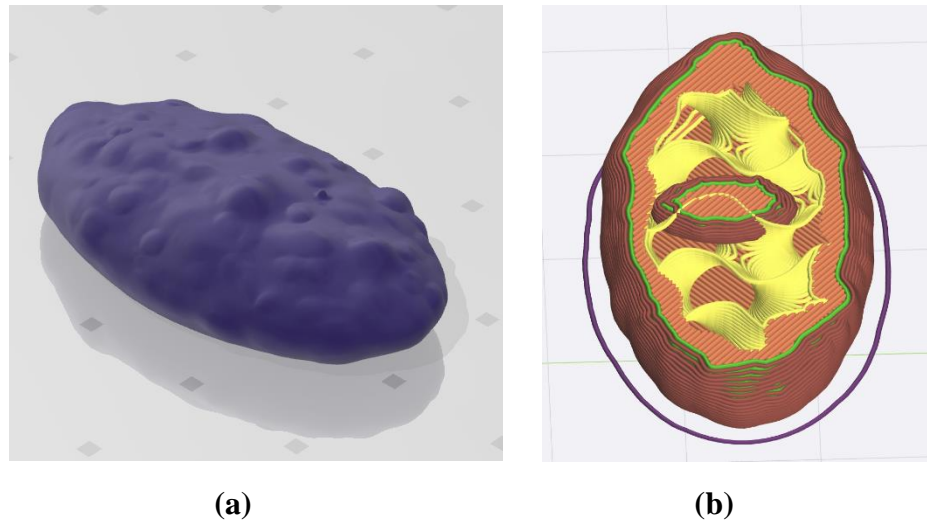


**Figure 38. (a) STL file of tonsil model [from JoePKrcma on Thingiverse.com]. (b) Model in 3D printing software with tumor located inside.**

A surrogate organ cutting pilot test was conducted with five participants that have academic and/or professional experience with anatomical dissection or the education of medical students. This pilot test aimed to assess the participants' reactions to performing surgical cuts into the 3D-printed surrogate organs. Each participant dissected a total of 12 printed models. This was achieved with three copies of four gyroidal infill percentages: 10%, 15%, 20%, and 25%. All the models were printed with 1 mm external wall thickness. Each of the three trials had the order of the four infills randomized to exclude bias from the results. A #22 scalpel blade was provided and changed between each participant. Each participant was instructed to make a maximum of two cuts per model. However, the cutting technique was left to the discretion of the participant. Once the cuts were made, the participants were asked a series of questions. Participants were asked to rate the ability to cut each infill percentage model in a scale ranging from 1 to 5, where a value of 5 signifies that the model was very easy to cut, while value of 1 indicates the model was very difficult to cut. Therefore, the infill percentage with the highest accumulated score was considered to have the best performance for the purposes of the test. At the end of the cutting tests, the participants were asked to give their range of agreement to the following statements:

S1. The prototypes are realistic enough models to use for educating students.

S2. Students will be able to dissect these models safely.

S3. These types of models will be useful as a teaching tool to educate students in the laboratory or classroom.

The participants were instructed to provide their answer using a scale ranging from (1) strongly disagree, (2) disagree, (3) neutral, (4) agree, and (5) strongly agree. The survey blank form is included in Appendix B.

The survey participants were recruited to gather a wide range of educators and anatomists with experience in fixed and unfixed cadaveric dissection, dissection techniques and methods currently taught to medical students. The expertise of participants included: Participant #1 is a pathology assistant professor with 16 years of experience with dissection of primarily unfixed tissue; Participant #2 is the vice-chair of and a professor in the Department of Anatomy with 28 years of experience dissecting primarily fixed tissue; Participant #3 is a pathologist assistant with 4 years of experience dissecting only unfixed tissues; Participant #4 is a professor in the pathology department with 25 years of experience dissecting primarily fixed tissues; Participant #5 is a teaching assistant professor in neuroscience with 15 years of experience dissecting primarily fixed tissues.

### **5.3 Surrogate Organ Cutting Pilot Test Results**

#### **5.3.1 Methods of Cutting**

Participant #1 used the belly of the scalpel blade and a ‘sawing motion’ to cut a 3-4 mm slice of the model perpendicular to the long axis, as this is typically taught in their classroom.

Participant one teaches many classes to medical students, where they are instructed to dissect fresh tissues. This technique can best be illustrated in Figure 39. Participant #2 also used the belly of the knife to cut the model to produce slices of the models.



**Figure 39. Method of cutting model with the belly of the blade and cutting into small slices.**

Participant #3 used the surgical cutting method to dissect the model, by making an initial puncture, then angling the scalpel at 45° for the rest of the cut, which can be seen in Figure 40. Participant #5 used a similar surgical cutting method to dissect the model. They made small, sliced cuts perpendicular to the long axis, similar to how Participant #1 did. They explained that this method is commonly used in their day-to-day work.



**Figure 40. Method of cutting model with 45 ° cut.**

Participant #4 used the belly of the blade for cutting the model, while making longitudinal and transverse cuts, seen in Figure 41. The participant explained that their many years of research background taught them to make these cuts to show large features in the organ.



**Figure 41. Method of cutting model with the belly of the blade, making longitudinal and transverse cuts.**

### 5.3.2 Results of Survey and Comments

The scores assigned by the participants to each infill were summed across the three trials to determine the total score for each model summarized in Table 23. The results of the survey concluded that the 15% and 20% are the best infill percentages for the tonsil model, both scoring a total of 54 points. The 25% infill scored 38 points, whereas the 10% scored 34 points. Participant #1 said that 10% and 25% were equally unsafe, as 10% deformed substantially under the pressure of the blade, while 25% required too much force to cut safely. Participant #2 expressed difficulty cutting through the outer wall of the model, expressing that more infill made it easier to cut. Participant #4 expressed that the horizontal and vertical axes required a very different cut effort, regardless of infill percentage.

**Table 23. Summed ease of cutability scores for each infill assigned by participant.**

Participant #	Infill %			
	10%	15%	20%	25%
1	5	10	11	5
2	9	9	12	12
3	7	10	10	8
4	5	11	10	4
5	8	14	11	9
<b>Total</b>	<b>34</b>	<b>54</b>	<b>54</b>	<b>38</b>

**Table 24. Assigned scores by participants for each statement.**

Statement	Participant #	Strongly Disagree	Disagree	Neutral	Agree	Strongly Agree
		1	2	3	4	5
S1	1					
	2					
	3					
	4					
	5					
S2	1					
	2					
	3					
	4					
	5					
S3	1					
	2					
	3					
	4					
	5					

In addition to the levels of agreement summarized in Table 24, the participants provided a series of comments to express their reactions to the statements and the experiment in general as summarized below:

- Statement S1, “*The prototypes are realistic enough models to use for educating students,*” received one rating of ‘strongly agree,’ two ratings of ‘agree,’ one rating of ‘neutral,’ and one rating of ‘disagree.’ Participants #1 and #3 also expressed that the current models are not

realistic enough at this stage. Participant #1 expressed a desire for a pink model exterior to make it more anatomically correct, with a contrasting interior color. Participant #3 explained that these models have too much of a 'plastic' feel at this stage, and that further work to find a more realistic material would significantly improve the model.

- Statement S2, "*Students will be able to dissect these models safely,*" received two ratings of 'strongly agree,' two ratings of 'agree,' and one rating of 'disagree.' Participant #1 explained that the infill percentages 10% and 25% were equally difficult and unsafe to cut. A similar observation was made by Participant #2. They verbalized that the 10% deformed too much under the scalpel blade, making it too hard to balance while holding the model, while the 25% infill simply required too much force to safely cut through.
- Finally, Statement S3, "*These types of models will be useful as a teaching tool to educate students in the lab/classroom,*" received three ratings of 'strongly agree' and two ratings of 'agree.' All participants agreed that these models will be useful as a teaching tool for students. Participant #1 expressed that synthetic organ models would allow the students to learn in the classroom, without going to the morgue nearly as often. They firmly believe the models would be beneficial to their classroom teaching, especially if the tumor location, size, and presence was randomized among models. Participant #3 said this would be very useful to give every student a hands-on model instead of simply observing the professor or sharing one specimen amongst six other students. Participant #4 teaches an online anatomy class and expressed how useful these models would be for students who are not able to be in the laboratory.

## Chapter 6. Main Observations and Concluding Remarks

### 6.1 Conclusions

In this work, the importance of cadaveric dissection in medical training was addressed, and shortcomings of cadaveric organs and commonly used porcine tissues were revealed. The development of 3D printed synthetic organs was proposed as a potential solution to address gaps in current solutions. Six candidate materials including five thermoplastic urethanes (TPUs) and one type of thermoplastic elastomer with Shore hardness ranging from 75A to 95A were selected for fusion deposition modeling (FDM) 3D-printing. Moreover, three resin materials with Shore hardness ranging from 39A to 80A were also identified as potential candidate materials. Different infill percentages and external layer print orientations were used in combination to explore possible prototype models that can be utilized for surrogate organ fabrication meeting Aim #1 *“Identify and select materials and infill percentages that are accessible and 3D printable to potentially mimic organ material”* presented in Chapter 1.

Material characterization tests were conducted to determine mechanical properties of candidate materials under different printing and loading configurations. The testing approach adopted for this study assessed the differences between candidate synthetic materials and mechanical properties of organs to determine similarities between properties. Standard tests included durometer testing, raw filament tensile testing, dog bone tensile testing, and compression testing. In addition to the standard characterization tests, custom tests and fixtures were developed and modeled to mimic actual basic laboratory dissection techniques to ensure that the collected data is applicable to medical training. These tests included scalpel puncture test, needle test, scalpel cutting test and friction test. All tests included materials with variations



of infill percentages and/or external print layer orientations. Thus, meeting Aim #2 “*Conduct mechanical characterization test of selected materials for different loading, infill percentages, and print layer orientations*” presented in Chapter 1.

Material characterization tests and the custom surgical tests described above were also performed on porcine and fixed and unfixed cadaver tissue to enable data comparison to synthetic materials. The data collected from these tests and data acquired from literature were used in conjunction to fulfill specific Aim #3 “*Compare experimental data to fixed and unfixed organs or tissues to determine similarities with 3D printed materials*” presented in Chapter 1.

The ‘best material’ for the purposes of this study was determined from the following criteria: (a) The synthetic material properties must closely compare to the tissue/organ data collected or obtained from literature; (b) If the synthetic material does not meet the requirements, then the best material will be the closest to the comparative data. As mentioned in the requirements of this study, the best material must also be 3D printable, accessible, and safe to cut with a scalpel. An overview of test results and main observations are presented below:

- The durometer test determined the true hardness of each candidate material. Materials were close to their manufacturer’s specified hardness except PFLX-95A with a difference of 8.7% and RFLX-82A with a percent difference of 4.2%, all other TPU and TPEs were less than 2% as presented in Table 3. The resin materials 50A and 39A were less accurate with percent differences of 14.6% and 105.4%, respectively, as presented in Table 4. The cadaveric tissue testing results showed that preserved (‘fixed’) organs were 26%-28% harder than unfixed organs. This determined that the hardest fixed organ is approximately 61% softer than the candidate TPU and TPE materials as presented in Table 5.

- Tensile testing filament data indicated that none of the candidate materials reached the breaking point elongations of the manufacturer's data, because they were not stretched nearly enough. For this work's purposes and intended use, the material did not need to be tested at its maximum elongation.
- The dog-bone specimen tensile tests showed that the closest matching material to the values reported in the literature was the NTEK-75A. For all print orientations, specimens printed with this relatively "soft" TPE compare best within a range from 7 MPa to 14 MPa (Table 7) to the 6 to 14 MPa (Table 8) range of the pig kidney from (Farshad et al. 1999). Most of the values found in the literature were generally lower than the measurements obtained from experimental testing. The smallest maximum stress value recorded from the collected data was the NFLX-83A, at 90° orientation with a strength of 5 MPa as presented in Table 7. Therefore, this material and orientation is determined the second best.
- The unconfined compression test determined that the NETK-75A material with 30% infill with a maximum stress value of 0.3 MPa (Table 9) was in the range of the Bosschetti et al. (2004) study. This material and infill were the only value in range of the literature data. Although the next materials that were slightly softer than the range were both NFLX-83A and RFLX-82A with 10% infill with a maximum stress of 0.2 MPa as presented in Table 9. These materials could potentially have values within this literature range if infills between 10% and 30% were attempted.
- The confined compression test results show that the closest value to the literature data comes from the 10% infills of all materials with a maximum stress of 0.3 MPa, except the NTEK-75A, with a 30% infill and maximum stress of 0.5 MPa as presented in Table 10.

- Scalpel puncture test results showed that the NTEK-75A with a 30% infill required the lowest force (2.6 N) to produce a puncture as presented in Table 11. The next closest material was the NFLX-83A with a 10% infill required 4.3 N to puncture the specimen. The results of the resin testing showed that the most comparable resin to filament would be the solid 50A resin and the 50% infill of the RFLX-82A or the PFLX-95A. Although to confirm this, a resin specimen with a specified infill will need to be re-tested, and not purely solid.
- The conclusions from the needle puncture indicated that the NTEK-75A with the 10% infill required the lowest force (4.3 N) to produce a puncture as presented in Table 13. The material with the next lowest force was the NFLX-83A with 10% infill, with a force of 7.9 N needed to produce a puncture.
- The following observations are extracted from the scalpel cutting tests:
  - For the first scalpel test configuration, 1 mm and 6 mm cutting depths with varying infills, the material that required the lowest average force to cut was the PFLX-95A 10% infill with force values of 10.4 N and 23.5 N, followed by NFLX-83A 10% infill with force of 10.6 N and 29.5 N, respectively, as presented in Table 16. This is likely due to the low friction of the PFLX-95A, and low stiffness, causing the material to deform under the scalpel blade, and not cutting through the material. This was observed on multiple specimens after the testing was completed.
  - For the second scalpel test configuration, 1 mm and 6 mm cutting depths with varying external print layer orientations and 4% infill, the material that required the lowest average force was the PFLX-95A for all print layer orientations averaging 3.6 N (Table 17) and 9.6 N (Table 18), respectively. The second material was the NFLX-83A for all

print layer orientations averaging 4.7 N (Table 17) and 20.3 N (Table 18), respectively.

The orientation that required the lowest force to cut was the 90° linear orientation.

- For the third scalpel test configuration, 1 mm cutting depth with varying external print layer orientations including perpendicular and parallel to the direction of the cut, with a 10% infill, the material that required the lowest average force to cut was the NFLX-83A for both orientations. This material required an average force of 3.1 N for the perpendicular cutting, and 2.5 N (for the parallel cutting directions) as presented in Table 19. Not all materials experienced a lower required cutting force in the parallel printing orientation as opposed to the perpendicular orientation. During these tests it was observed that the blade began to deflect resulting in cross cutting of print layers and altering the required cutting force. An example of this can be seen in Figure 34.
- The cutting tests with resin materials compared to TPU/TPE with the #22 blade, showed that Resin 50A Resin 80A had the closest values to the TPU/TPE averaging 10.5 N and 14.1 N required to cut, respectively, as presented in Table 20. Cutting tests with the #11 blade showed a required a lower cutting force, 7.4 N and 6.4 N, for both the Resin 50A and the Resin 80A, respectively, which resulted in a 54.6% and 29.5% percent difference between the two blade types (Table 20).
- The friction test revealed that the NFLX-83A had the lowest static friction coefficient (0.38) and PFLX-95A produced the highest static friction coefficient (0.91) as presented in Tables 22 and 23. PFLX-95A experienced a 5.4% difference between the print layer directions followed by NFLX-85A with a 1.4% difference, NFLX-83A with a -3.3% difference, and finally RFLX-82A with the largest difference of -28.1%.

The results of every mechanical test indicated that all the candidate materials were relatively “stiffer” than tissue material properties reported in the literature. Despite this limitation, a ‘best material’ that exhibited the lowest required cutting force was deemed the best material for the purposes of this study. The custom designed tests for this application were more useful in determining the best infill percentage and combination of material. As the raw tensile test was merely to verify the properties reported by the material’s manufacturer. The scalpel cutting test, and the scalpel puncture test were the two most important tests in determining the force required to make an incision by the technique mentioned in Kirk (2002).

Overall, the 10% infill was the closest in comparison to organ tissue data, although results obtained in this study show this was still too stiff. However, the combination of 10% infill with softer materials can potentially give a mechanical behavior comparable to real organs. The closest material overall was the NTEK-75A with a 10% infill. As testing continued, and due to its inherent flexibility and low hardness, this material exhibited difficulty for reliable and consistent printing of the different specimens required for the tests. Therefore, a more reliable material was needed and was found by selecting the next best material determined from the tests. Thus, the material chosen was the NFLX-83A, as it performed best under the required use conditions. Once the best material was determined, a small surrogate model was printed with four different infills of 10%, 15%, 20%, and 25% and used to conduct a pilot surgical cutting test. A group of five anatomists were recruited to conduct cutting tests and later responded to a survey to determine the best infill percentage for the final surrogate organ, and overall thoughts about the model. The highest scores corresponded to infill percentages in the range of 15% to 20%. The overall feedback of the survey determined that the synthetic models will be useful as a teaching tool to educate medical students, although additional work is needed to improve safety

during cutting, as well as improvements in the selection of materials and printing parameters to better mimic real organs. This series of surgical cutting tests conducted by specialists met specific Aim #4 “*Conduct a survey with anatomists determining their opinions on the overall final surrogate organ, material, and infill percentage*” presented in Chapter 1.

## **6.2 Study Limitations and Future Work**

The list of improvements in this research that can be made with some additional testing and modifications are as follows:

- The best material for the applications envisioned in this study was determined to be the NTEK-75A, a relatively flexible and “soft” TPE that displayed acceptable mechanical properties for the purposes of this study. However, its printability was unreliable. Thus, addressing the printing reliability issues would allow expanded use of this material and ultimately obtain a better educational model. Once this printing issue is corrected, the tests presented in this study without this material should be done for the NTEK-75A.
- Resin 50A and Resin 80A both demonstrated the potential to be made into a softer synthetic material by using software that allows infill generation within the resin specimens. Further research may permit a more realistic and smoother surrogate specimen than those obtained with FDM printing.
- The glove and synthetic material friction testing was conducted under dry conditions. Often, when handling cadaveric or fresh organs, bodily fluids or preservation fluids on the outside surface of the organs and tissues provide a natural lubricant, creating a more complicated handling process. Thus, friction tests under a wet glove condition would create a more

realistic scenario for handling surrogate 3D-printed organs, although the dry conditions are suitable for this application.

- The correlation between the experimental results obtained from the customized tests and the participants' experience captured in surveys needs to be quantified more precisely. Developing a numerical relationship will allow more precise quantification of the performance of each candidate material in relation to the intended user experience.
- Finally, while gyroidal infill provided a good starting approximation to the organ's internal structure, considering other infill geometries and configurations that can reproduce a more realistic anatomical internal structure would allow the development of a more accurate surrogate model that can be used for training medical students.

## 9. References

- 3Dprinting. 2023. “Silicone 3D Printing.” <https://3dprinting.com/3d-printing-use-cases/an-overview-of-silicone-3d-printing/> (November 23, 2023)
- “Annexes A-D.” 2009. *Annals of the ICRP* 39(2): 47–70.
- ASTM D638-14. 2022. *Test Method for Tensile Properties of Plastics*. ASTM International. <http://www.astm.org/cgi-bin/resolver.cgi?D638-14> (May 9, 2023).
- ASTM D695-15. 2015. *Test Method for Compressive Properties of Rigid Plastics*. ASTM International. <http://www.astm.org/cgi-bin/resolver.cgi?D695-15> (May 9, 2023).
- ASTM D1894. 2011. *Test Method for Static and Kinetic Coefficients of Friction of Plastic Film and Sheeting*. ASTM International. <http://www.astm.org/cgi-bin/resolver.cgi?D1894-14> (July 19, 2023).
- ASTM D2240-15. 2021. *Test Method for Rubber Property Durometer Hardness*. ASTM International. <http://www.astm.org/cgi-bin/resolver.cgi?D2240-15R21> (October 16, 2023).
- ASTM F1342. 2022. *Test Method for Protective Clothing Material Resistance to Puncture*. ASTM International. <http://www.astm.org/cgi-bin/resolver.cgi?F1342F1342M-05R22> (May 29, 2023).
- BCN3D. 2023. “BCN3D Slicing Guide 3: Wrap Your Head around Wall Thickness.” <https://www.bcn3d.com/bcn3d-x-flowalistik-slicing-guide-3-wall-thickness/>.
- Boschetti, Federica, Giancarlo Pennati, and Francesca Gervaso. 2004. “Biomechanical Properties of Human Articular Cartilage under Compressive Loads.” *Biorheology* 41: 159–66.
- Brownell, Lindsay. 2019. “A Swifter Way towards 3D-Printed Organs.” <https://wyss.harvard.edu/news/a-swifter-way-towards-3d-printed-organs/>.
- Brunon, A., K. Bruyère-Garnier, and M. Coret. 2010. “Mechanical Characterization of Liver Capsule through Uniaxial Quasi-Static Tensile Tests until Failure.” *Journal of Biomechanics* 43(11): 2221–27.
- Buj-Corral, Irene, Alejandro Domínguez-Fernández, and Ramón Durán-Llucià. 2019. “Influence of Print Orientation on Surface Roughness in Fused Deposition Modeling (FDM) Processes.” *Materials* 12(23): 3834.
- Cabreira, Vinicius, and Ruth Marlene Campomanes Santana. 2020. “Effect of Infill Pattern in Fused Filament Fabrication (FFF) 3D Printing on Materials Performance.” *Matéria (Rio de Janeiro)* 25(3): e-12826.



- Chandra, Somodyuti, Indrashis Podder, Manas Chatterjee, and Lawrence Field. 2018. “Anatomy and Applications of the #15 Scalpel Blade and Its Variations.” *Journal of Cutaneous and Aesthetic Surgery* 11(2): 79.
- Chanthasopephan, T., J.P. Desai, and A.C.W. Lau. 2006. “Determining Fracture Characteristics in Scalpel Cutting of Soft Tissue.” In *The First IEEE/RAS-EMBS International Conference on Biomedical Robotics and Biomechanics, 2006. BioRob 2006.*, Pisa, Italy: IEEE, 899–904. <http://ieeexplore.ieee.org/document/1639205/> (May 9, 2023).
- Chu, Jennifer. 2023. “Custom, 3D-Printed Heart Replicas Look and Pump Just like the Real Thing.” <https://news.mit.edu/2023/custom-3d-printed-heart-replicas-patient-specific-0222>.
- De Bazelaire, Cedric. 2009. “Blunt-Tip Coaxial Introducer: A Revisited Tool for Difficult CT-Guided Biopsy in the Chest and Abdomen.” *American Journal of Roentgenology* 193(2): W144–48.
- Farshad, Mehdi. 1999. “Material Characterization of the Pig Kidney in Relation with the Biomechanical Analysis of Renal Trauma.” *Journal of Biomechanics* 32(4): 417–25.
- Formlabs. 2023. “FDM vs. SLA: Compare Filament and Resin 3D Printers.” <https://formlabs.com/blog/fdm-vs-sla-compare-types-of-3d-printers/>.
- Forster, Aaron M. 2015. *Materials Testing Standards for Additive Manufacturing of Polymer Materials: State of the Art and Standards Applicability*. National Institute of Standards and Technology. <https://nvlpubs.nist.gov/nistpubs/ir/2015/NIST.IR.8059.pdf> (May 9, 2023).
- Garcia, Justine. 2018. “3D Printing Materials and Their Use in Medical Education: A Review of Current Technology and Trends for the Future.” *BMJ Simulation and Technology Enhanced Learning* 4(1): 27–40.
- Gerostamoulos, Dimitri, and Jennifer Schumann. 2023. “Postmortem Specimens.” In *Encyclopedia of Forensic Sciences, Third Edition*, Elsevier, 246–53. <https://linkinghub.elsevier.com/retrieve/pii/B9780128236772002762> (June 12, 2023).
- Goshen College. 2004. “Human/Pig Comparisons.” <https://www.goshen.edu/academics/biology/pigbook/human-pig-comparisons/#:~:text=of%20the%20FPDG-,Internal%20Organs,%2C%20left%20lateral%2C%20and%20caudate>.
- Hollenstein, Marc. 2006. “Mechanical Characterization of the Liver Capsule and Parenchyma.” In *Biomedical Simulation, Lecture Notes in Computer Science*, eds. Matthias Harders and Gábor Székely. Berlin, Heidelberg: Springer Berlin Heidelberg, 150–58. [http://link.springer.com/10.1007/11790273\\_17](http://link.springer.com/10.1007/11790273_17) (August 19, 2023).
- Horvath, Joan. 2014. *Mastering 3D Printing*.

- Kirk, R M. 2002. *Basic Surgical Techniques*. 5th ed. London UK: Churchill Livingstone.
- Koiter, W. T. 1945. "On the stability of elastic equilibrium." PhD thesis, Technische Hogeschool Technological University of Delft, Delft, Holland.
- Letcher, Todd, and Megan Waytashek. 2014. "Material Property Testing of 3D-Printed Specimen in PLA on an Entry-Level 3D Printer." In *Volume 2A: Advanced Manufacturing*, Montreal, Quebec, Canada: American Society of Mechanical Engineers, V02AT02A014.  
<https://asmedigitalcollection.asme.org/IMECE/proceedings/IMECE2014/46438/Montreal,%20Quebec,%20Canada/262371> (May 9, 2023).
- Maurin, B. 2004. "In Vivio Study of Forces during Needle Insertions." In *Perspective in Image-Guided Surgery*, RheinAhrCampus Remagen, Germany: WORLD SCIENTIFIC, 415–22.  
[http://www.worldscientific.com/doi/abs/10.1142/9789812702678\\_0056](http://www.worldscientific.com/doi/abs/10.1142/9789812702678_0056) (June 25, 2023).
- Ntonas, Athanasios. 2020. "Comparative Anatomical Study Between the Human and Swine Liver and Its Importance in Xenotransplantation." *Cureus*.  
<https://www.cureus.com/articles/34044-comparative-anatomical-study-between-the-human-and-swine-liver-and-its-importance-in-xenotransplantation> (May 25, 2023).
- Oviedo, A.M., A.H. Puente, C. Bernal, and E. Pérez. 2020. "Mechanical Evaluation of Polymeric Filaments and Their Corresponding 3D Printed Samples." *Polymer Testing* 88: 106561.
- Princeton University. "Using Sharps Safely in the Research Laboratory."  
<https://ehs.princeton.edu/laboratory-research/biological-safety/biosafety-manual/using-sharps-safely>.
- Prodex Profiles Elastomeres. "Shore Hardness Essentials." <https://en.prodex-elastomeres.com/practical-handbook/shore-hardness/>.
- Qi, H. J., K. Joyce, and M. C. Boyce. 2003. "Durometer Hardness and the Stress-Strain Behavior of Elastomeric Materials." *Rubber Chemistry and Technology* 76(2): 419–35.
- Radenkovic, Dina, Atefeh Solouk, and Alexander Seifalian. 2016. "Personalized Development of Human Organs Using 3D Printing Technology." *Medical Hypotheses* 87: 30–33.
- Singh, Poonam, Naveen Phuyal, Sagar Khadka, and Minani Gurung. 2021. "Knowledge of Medical Students and Faculties of a Medical College Towards Human Body and Organ Donation: A Descriptive Cross-Sectional Study." *Journal of Nepal Medical Association* 59(234). <http://www.jnma.com.np/jnma/index.php/jnma/article/view/6200> (June 13, 2023).
- Smooth-On. 2023. "Durometer Shore Hardness Scale." <https://www.smooth-on.com/page/durometer-shore-hardness-scale/>.

- Snedeker, J.G. 2005. “Strain-Rate Dependent Material Properties of the Porcine and Human Kidney Capsule.” *Journal of Biomechanics* 38(5): 1011–21.
- Spagnoli, A., R. Brighenti, M. Terzano, and F. Artoni. 2019. “Cutting Resistance of Soft Materials: Effects of Blade Inclination and Friction.” *Theoretical and Applied Fracture Mechanics* 101: 200–206.
- Stingl, J. 2002. “Morphology and Some Biomechanical Properties of Human Liver and Spleen.” *Surgical and Radiologic Anatomy* 24(5): 285–89.
- Su, Amanda, and Subhi J. Al’Aref. 2018. “History of 3D Printing.” In *3D Printing Applications in Cardiovascular Medicine*, Elsevier, 1–10.  
<https://linkinghub.elsevier.com/retrieve/pii/B9780128039175000018> (June 1, 2023).
- Suaste-Gómez, Ernesto, Grissel Rodríguez-Roldán, Héctor Reyes-Cruz, and Omar Terán-Jiménez. 2016. “Developing an Ear Prosthesis Fabricated in Polyvinylidene Fluoride by a 3D Printer with Sensory Intrinsic Properties of Pressure and Temperature.” *Sensors* 16(3): 332.
- Tan, Eddie T. W., Ji Min Ling, and Shree Kumar Dinesh. 2016. “The Feasibility of Producing Patient-Specific Acrylic Cranioplasty Implants with a Low-Cost 3D Printer.” *Journal of Neurosurgery* 124(5): 1531–37.
- The Engineering ToolBox. “Friction Coefficients and Calculator.”  
[https://www.engineeringtoolbox.com/amp/friction-coefficients-d\\_778.html](https://www.engineeringtoolbox.com/amp/friction-coefficients-d_778.html).
- Timoshenko, J. 1914. “Towards the question of deformation and stability of cylindrical shell.” *Vesti Obshestva Tekhnologii*, 21: 785-792.
- University of Illinois. 1945. “The Chemical Composition of the Adult Human Body and Its Bearing on the Biochemistry of Growth.”
- USA Medical and Surgical Supplies. 2018. “Surgical Blades: Which Scalpels Are Right for Your Operating Room?” <https://www.usamedicalsurgical.com/blog/surgical-blades-which-scalpel-is-right-for-your-operating-room>.
- Wilts, Bodo D. 2017. “Butterfly Gyroid Nanostructures as a Time-Frozen Glimpse of Intracellular Membrane Development.” *Science Advances* 3(4): e1603119.
- Xia, Tingting, Wanqian Liu, and Li Yang. 2017. “A Review of Gradient Stiffness Hydrogels Used in Tissue Engineering and Regenerative Medicine: GRADIENT STIFFNESS HYDROGELS USED IN TISSUE ENGINEERING AND REGENERATIVE MEDICINE.” *Journal of Biomedical Materials Research Part A* 105(6): 1799–1812.
- Xometry. 2022. “TPE vs. TPU: Differences and Comparison.”  
<https://www.xometry.com/resources/3d-printing/tpe-vs-tpu-3d-printing/>.

Yoon, Young Chul 2017. "Quantitative Assessment of Liver Fibrosis Using Shore Durometer."  
*Annals of Surgical Treatment and Research* 93(6): 300.

## 8. Appendix A

Copyright Notice: All technical data sheets are owned by the manufacturer and are copyrighted.

### Raise3D Premium TPU-95A Technical Data Sheet

Raise3D Premium TPU-95A (Thermoplastic polyurethane) is a flexible and elastic 3D printing filament. Its rubber-like elasticity, resilience, and durability make it suitable for uses requiring impact-absorption and a soft-touch surface. TPU-95A printed parts are widely used in applications such as insoles, tubes, seals, and bushings.

#### Physical Properties

Property	Testing Method	Typical Value
Density (g/cm <sup>3</sup> )	ISO 1183 (at 21.5 °C)	1.20 - 1.24
Melt index (g/10 min)	ISO 1133 (210 °C, 1.2 kg)	3 - 6
Moisture content <sup>1</sup> (%)	Thermogravimetric	≤ 0.1%
Odor	/	Almost odorless
Solubility	/	Insoluble in water

1. For newly opened filaments; filaments may absorb higher levels of moisture during use.

#### Mechanical Properties<sup>1</sup>

Property	Testing Method	Typical Value
Young's modulus (MPa)	ISO 37	9.5 ± 0.4
Tensile strength (MPa)	ISO 37	29.3 ± 2.8
Elongation at break (%)	ISO 37	330 ± 15
Shore Hardness	ISO 7619	95A

1. All testing specimens were printed using a Raise3D Pro 2 under the following conditions:

Printing temperature = 255 °C, printing speed = 30 mm/s, number of shells = 2, and 100% infill.

All specimens were conditioned at room temperature for 24h prior to testing.

**Figure 42. R3D-95A Technical data sheet (Raise3D, 'Raise3D Premium TPU-95A Technical Data Sheet', June 2021)**

## PolyFlex™ TPU95

PolyFlex™ TPU95 is a thermoplastic polyurethane (TPU) based filament specifically engineered to work on most desktop 3D printers. It has a shore hardness of 95A and can stretch more than 3 times its original length.

### Physical Properties

Property	Testing method	Typical value
Density	ASTM D792 (ISO 1183, GB/T 1033)	1.20 - 1.24 (g/cm <sup>3</sup> at 21.5 °C)
Melt index	210 °C, 1.2 kg	3-6 (g/10 min)

Tested with 3D printed specimen of 100% infill

### Mechanical Properties

Property	Testing method	Typical value
100% modulus (X-Y)	ASTM D638 (ISO 527, GB/T 1040)	9.4 ± 0.3 (MPa)
Tensile strength (X-Y)	ASTM D638 (ISO 527, GB/T 1040)	29.0 ± 2.8 (MPa)
Elongation at break (X-Y)	ASTM D638 (ISO 527, GB/T 1040)	330.1 ± 14.9 (%)
Shore hardness	ASTM D2240 (ISO 7619, GB/T 31)	-95A

All testing specimens were printed under the following conditions:  
 nozzle temperature = 225 °C, printing speed = 30 mm/s, build plate temperature = 30 °C, infill = 100%  
 All specimens were conditioned at room temperature for 24h prior to testing

### Recommended printing conditions

Parameter	
Nozzle temperature	210 - 230 (°C)
Build Surface material	BuildTak®, Glass, Blue Tape
Build surface treatment	None, Applying PVA glue to the build surface
Build plate temperature	25 - 60 (°C)
Cooling fan	Turned on
Printing speed	20-40 (mm/s)
Raft separation distance	0.2 (mm)
Retraction distance	1 (mm)
Retraction speed	20 (mm/s)
Recommended environmental temperature	Room temperature - 45 (°C)
Threshold overhang angle	35 (°)
Recommended support material	PolySupport™ and PolyDissolve™ S1

Based on 0.4 mm nozzle and Simplify 3D v.3.1. Printing conditions may vary with different nozzle diameters

**Figure 43. PFLX-95A Technical data sheet (Polymaker, ‘PolyFlex TPU95A Technical Data Sheet’, November 2018)**

## NinjaFlex® 3D Printing Filament

### Flexible Polyurethane Material for FDM Printers

NinjaFlex flexible filament leads the industry with superior flexibility and longevity compared to non-polyurethane materials. Its consistency in diameter and ovality (roundness) outpaces other polyurethane materials. Made from a specially formulated thermoplastic polyurethane (TPU) material, this patented technology contains a low-tack, easy-to-feed texture. The result is uniquely flexible, strong prints ideal for direct-drive extruders.

General Properties	Test Method	Imperial	Metric
Specific Gravity	ASTM D792	1.19 g/cc	1.19 g/cc
Moisture Absorption - 24 hours	ASTM D570	0.22 %	0.22 %

Mechanical Properties	Test Method	Imperial	Metric
Tensile Strength, Yield	ASTM D638	580 psi	4 Mpa
Tensile Strength, Ultimate	ASTM D638	3,700 psi	26 Mpa
Tensile Modulus	ASTM D638	1,800 psi	12 Mpa
Elongation at Yield	ASTM D638	65%	65%
Elongation at Break	ASTM D638	660%	660%
Toughness (integrated stress-strain curve; calculated stress x strain)	ASTM D638	12,000 in-lbf/in <sup>2</sup>	82.7 m <sup>2</sup> N/m <sup>2</sup> x10 <sup>6</sup>
Hardness	ASTM D2240	85 Shore A	85 Shore A
Impact Strength (notched Izod, 23C)	ASTM D256	2.0 ft.lbf/in <sup>2</sup>	4.2 kJ/m <sup>2</sup>
Abrasion Resistance (mass loss, 10,000 cycles)	ASTM D4060	0.08 g	0.08 g

Thermal Properties	Test Method	Imperial	Metric
Melting Point (via Differential Scanning Calorimeter)	DSC	420° F	216° C
Glass Transition (Tg)	DSC	-31° F	-35° C
Heat Deflection Temperature (HDT) @ 10.75psi/ 0.07 MPa	ASTM D648	140° F	60° C
Heat Deflection Temperature (HDT) @ 66psi/ 0.45 MPa	ASTM D648	111° F	44° C

NinjaFlex filament is capable of being printed by a variety of printers in a variety of configurations. This specification sheet gives results as they pertain to the defined test standard and specimen details. Different slicing and/or printing configurations, test conditions, ambient environments, etc. may result in different results.

Impact Strength and Heat Deflection Temperature results were both provided by an accredited university testing laboratory. Specific Gravity and Hardness are innate characteristics of the material. Moisture Absorption, values associated with the Tensile Strength tests, Melting Point and Glass Transition data were prepared by Fenner Drives, Inc.

NinjaFlex makes no warranties of any type, express or implied, including, but not limited to, the warranties of fitness for a particular application.

**Test Specimen Details (By ASTM Test Number)**

All printed specimens were created using the T122 printer 0.75mm nozzle. For ASTM D638 tests, the reduction multiplier is 1.03.

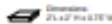
**Specific Gravity (D792):** Results determined by nature of material.

**Moisture (D570):** 30g of filament tested in moisture analyzer evaluated at 120°C until the mass change is < 0.0005% over 1 minute.

**Tensile (D638):** Dogbone Style (C) 100% fil, diagonal line fit. Dimensions: 3mm thick. See drawing for other dimensions.



**Hardness (D2240):** Solid testing block.



**Impact (D256):** Un-notched test specimen, notch added post print by testing facility.

Dimensions: 28.1 x 6.35 mm x 6.35 mm

**Abrasion (D4060):** Rectangular block sized to fit labar abrader.

Dimensions: 6.35 x 6.35 mm x 6.35 mm

**HDT (D648):** Notched.

Dimensions: 10.16 x 6.35 mm x 6.35 mm

Figure 44. NFLX-85A Technical data sheet (NinjaTek, ‘NinjaFlex 3D Printing Filament’, April 2016)

## NinjaFlex® Edge 3D Printing Filament

### Flexible Material for FDM Printers

NinjaFlex Edge flexible filament leads the industry with superior flexibility and longevity compared to competitors. Its consistency in diameter and ovality (roundness) outpaces other materials. Made from a specially formulated thermoplastic material, this patented technology contains a low-tack, easy-to-feed texture. The result is uniquely flexible, strong prints ideal for extruders.

General Properties	Test Method	Imperial	Metric
Specific Gravity	ISO 1183	1.08 g/cc	1.08 g/cc
Moisture Absorption - 24 hours	ISO 62	0.8 %	0.8 %
Mechanical Properties			
Tensile Strength, Ultimate	ISO 527-2	2180 psi	13.9 Mpa
Tensile Modulus	ISO 527-1	3630 psi	25 Mpa
Elongation at Break	ISO 527-2	900%	900%
Hardness	ISO 868	83 Shore A	83 Shore A
Thermal Properties			
Melting Point (via Differential Scanning Calorimeter)	ISO 11357	356° F	180° C
Glass Transition (Tg)	ISO 11357	-112° F	-80° C

**Figure 45. NFLX-83A Technical data sheet sheet (NinjaTek, ‘NinjaFlex Edge 3D Printing Filament’, March 2020)**



# FilaFlex

THE ORIGINAL ELASTIC FILAMENT FOR 3D PRINTING

PROPERTIES	STANDARD	VALUE	UNIT	TEST CONDITION
Shore hardness, method A	ISO 868	82	SHORE A	
Ultimate tensile strength	DIN 53504	54	Mpa	
Elongation to break	DIN 53504	700	%	200 mm/min
Compression set	ISO 815	25	%	72 h; 23 °C
Impact resilience	ISO 4662	42	%	
Abrasion resistance	ISO 4649 method A	30	mm <sup>3</sup>	
Tear propagation resistance	ISO 34-1	70	kN/m	500mm/min
Density	ISO 1183-1	1200	kg/m <sup>3</sup>	
Tensile storage modulus	ISO 6721-1,-4	48	MPa	20 °C
Tensile storage modulus	ISO 6721-1,-5	33	MPa	60 °C
Extrusion-Melt Temperature		200-260	°C	

## CONSIDERATIONS

Filaflex *is not a Medical grade material*, cannot be used with direct contact with body fluids including direct contact with blood

Filaflex *is not designated to food contact or cosmetics applications.*

Figure 46. RFLX-82A Technical data sheet sheet (FilaFlex, ‘Recreus Technical Data Sheet, March 2018)

## Chinchilla™ 3D Printing Filament

Flexible TPE Material for FDM Printers

Chinchilla™ flexible 3D printer filament is the softest, best-feeling matte material in the market today. Created through a combination of premium TPE resins, Chinchilla's proprietary blend provides rebound, impact resistance and durability. With Chinchilla, you can create soft, long-lasting printed parts for fashion, healthcare and more.

General Properties	Test Method	Imperial	Metric
Specific Gravity	ASTM D792	1.13 g/cc	1.13 g/cc
Moisture Absorption - 24 hours	ASTM D570	0.8 %	0.8 %

Mechanical Properties	Test Method	Imperial	Metric
Tensile Strength, Yield	ASTM D638	770 psi	5 Mpa
Tensile Strength, Ultimate	ASTM D638	3,189 psi	22 Mpa
Tensile Modulus	ASTM D638	4,995 psi	34 Mpa
Elongation at Yield	ASTM D638	20%	20%
Elongation at Break	ASTM D638	600%	600%
Hardness	ASTM D2240	75 Shore A	75 Shore A

Thermal Properties	Test Method	Imperial	Metric
Melting Point	DSC	356° F	180° C
Glass Transition (Tg)	DSC	-12° F	-80° C

NinjaTek filament is capable of being printed by a variety of printers in a variety of configurations. This specification sheet gives results as they pertain to the defined test standard and specimen details. Different slicing and/or printing configurations, test conditions, ambient environments, etc. may result in different results.

NinjaTek makes no warranties of any type, express or implied, including, but not limited to, the warranties of fitness for a particular application.

**Figure 47. NTEK-75A Technical data sheet sheet (NinjaTek, ‘Chinchilla 3D Printing Filament’, March 2021)**

## 9. Appendix B

### Surrogate Organ Cutting: Pilot Test

#### Post-Testing Survey

Instructions:

This pilot test aims to assess participants' reactions to performing surgical cuts into 3D-printed surrogate organs being developed for the educational purposes of medical students. The participants of this test will consist of subjects with academic and/or professional experience with anatomical dissection and the education of medical students.

Each participant will be given 12 synthetic prototypes of one organ. The 12 models will include three copies of the same prototype 3D printed with four infill levels (10%, 15%, 20%, and 25%). The higher the percentage, the higher the volumetric density of the material inside the model, which changes its cutability. Each model contains a small tumor-like insert inside the specimen made of a different material. A scalpel blade will be provided to the participant, who will be instructed to make a maximum of 2 cuts per model. Once the cuts have been made, the participant will be asked the following questions.

Assessment	Strongly Disagree	Disagree	Neutral	Agree	Strongly Agree
Scale	1	2	3	4	5
Q1. The prototypes are realistic enough models to use for educating students.					
Q2. Students will be able to dissect these models safely.					
Q3. These type of models will be useful as a teaching tool to educate students in the lab/classroom.					

Please rank each infill percentage model on its ability to be cut.

Assessment	Very Easy	Easy	Somewhat Difficult	Difficult	Very Difficult
Scale	5	4	3	2	1
10% Infill Model					
15% Infill Model					
20% Infill Model					
25% Infill Model					

Additional Comments:

---



---



---

**Figure 48. Surrogate organ cutting pilot test.**